



# Quasinormal Modes of Non-Linearly Charged Black Holes surrounded by a Cloud of Strings in Rastall Gravity

Dhruba Jyoti Gogoi <sup>\*</sup>, Ronit Karmakar,<sup>†</sup> and Umananda Dev Goswami <sup>‡</sup>  
*Department of Physics, Dibrugarh University, Dibrugarh 786004, Assam, India*

We obtain the black hole solution for the Ayón - Beato - García (ABG) type black hole surrounded by a cloud of strings in Rastall gravity and calculate the scalar quasinormal modes of it for a massless scalar field. To have a better visualization of the results, we also introduce a new non-linear electrodynamic source and obtain a black hole solution surrounded by a cloud of strings in the Rastall gravity. We see that the quasinormal modes are affected by the type of non-linear electrodynamic sources in case of higher magnitudes of charge  $q$ . With increase in the magnitude of charge  $q$ , gravitational waves decay rapidly for the new black hole solution, while for the ABG black hole, the decay rate increases initially and finally starts to decrease near to  $q = 1$ . We also study the impact of the cloud of strings and other model parameters, including the Rastall parameter on the quasinormal modes for both of the black holes. The gravitational waves decay slowly with increase in the cloud of strings parameter for both of the black holes. Dependency of quasinormal modes on the Rastall parameter is different from a surrounding dark energy field and the decay of gravitational waves may be slow or rapid depending on the value of this parameter.

PACS numbers:

Keywords: Modified Gravity; Gravitational Waves; Quasinormal modes; Black holes

## I. INTRODUCTION

The theory of General Relativity (GR) is widely regarded as the most elegant theory ever conceived. This beautiful theory has been put to test for many times in the past but it has emerged out to be consistent with experimental observations to a fair extent in most of the cases [1–3]. The most recent outstanding evidence in favour of GR came in the form of observations from the Laser Interferometer Gravitational Wave Observatory (LIGO) and the Variability of Solar Irradiance and Gravity Oscillations (Virgo), when they reported the first ever detection of Gravitational Waves (GWs) from the merger of two black holes in 2015 [4]. After that, many other events of GWs were detected by these observatories in the following years [5–11]. These detections have opened up a new research avenue to study the universe via GW astronomy. They also provide a testing ground for various theories of gravity including GR in the extreme gravity regime. Overall, GR has drastically uplifted our level of understanding and way of thinking about the universe – its origin, existence and future. However, GR was already known to have many drawbacks. Such as, in GR there is no scope for explaining the cosmic accelerated expansion [12, 13]. At a highly relativistic regime, GR is non-renormalizable [14] and at some stage, we have to encounter infinities in the theory. GR also does not provide any prediction regarding the dark components of the universe, whose presence has been indirectly shown by observations [15, 16]. Realizing these drawbacks, there have been attempts to modify GR.

The simplest modification of GR that includes the dark components of the observable universe in the form of some supplementary fields, which is most favorable in terms of cosmological observations at present, is the  $\Lambda$ CDM ( $\Lambda$  Cold Dark Matter) model. According to this model the universe is spatially flat, homogeneous and isotropic over the large scales, and is filled with a constant energy density fluid throughout, known as the cosmological constant  $\Lambda$  [17, 18]. This simple model fits well with almost all observational data that we have. But, it too has some drawbacks, e.g.,  $\Lambda$ CDM model is not able to justify the existence of  $\Lambda$ . Similarly,  $\Lambda$ CDM model fails to address the small value of  $\Lambda$  and hence the fine-tuning problem with the theoretical prediction. This represents the largest discrepancy between observed and theoretical predictions in the history of theoretical physics [18]. Moreover, there is no explanation for the constant energy density of the  $\Lambda$ , in contrast to the variation of energy density of the other components of the universe with the scale factor [18, 19]. To deal with these serious issues, different Modified Theories of Gravity (MTGs) were introduced, so that without introducing the dark components of the universe, this class of theories can predict observational data like accelerated expansion of the universe and the galactic rotation curves. Another key aspect to study in MTGs is the GWs, which has been studied vigorously in the past few decades and has been benefited from the endeavours to develop new MTGs [20, 21]. Various novel properties of GWs have emerged from the application of various MTGs. As an example, the presence of three polarization modes of GWs in metric formalism of  $f(R)$  theory opens up new

---

\*Email: [moloydhruba@yahoo.in](mailto:moloydhruba@yahoo.in)

†Email: [ronit.karmakar622@gmail.com](mailto:ronit.karmakar622@gmail.com)

‡Email: [umananda2@gmail.com](mailto:umananda2@gmail.com)

possibilities in GW observations. Here, two modes are the GR modes and the third mode is the scalar polarization mode, which consist of a combination of a massive longitudinal mode and a massless breathing mode [20, 22]. This has inspired a surge in research in this field, especially, the applications of new MTGs to black holes and stellar dynamics, and that lead to results predicting deviations from GR [20, 22, 23]. One may note that the extra polarization modes of GWs have been constrained by recent observations [24]. Particularly, the LIGO-Virgo collaboration gives the current bound on the mass of the quanta of massive mode, the graviton as  $m_g \leq 7.7 \times 10^{-23} \text{ eV}/c^2$  [25].

Among the modified theories, a special modification to GR was given by P. Rastall in 1972, where he proposed that the covariant derivative of the energy-momentum tensor does not vanish in curved spacetime, or in presence of massive objects, but only vanish in flat spacetime. This new model of gravity was called the Rastall gravity [26]. Recently, it has drawn the attention of researchers mainly due to the unique behaviour of violation of energy conservation in presence of background curvature. In this model, Rastall proposed the covariant derivative of the energy-momentum tensor to be equal to divergence of the Ricci scalar or curvature scalar  $R$ . However, the Bianchi identity of the vanishing divergence of the Einstein tensor was maintained [27]. It is to be noted that although the violation of conservation principle is shown exclusively by the Rastall theory only, but the same feature also includes inherently by other theories like  $f(R, T)$  theory and  $f(R, L_M)$  theory [27, 28]. This feature of Rastall gravity caused significant deviations from GR, specially near the high curvature regimes, like in the regions near the Black Holes and Neutron stars. Although Rastall gravity may be equivalent to GR in some aspects [29], one can see that in presence of non-zero curvature or some dark energy fields the theory can show significant deviations from GR [30]. Recently, a lot of important applications of Rastall theory can be seen in the literature, some of which includes gravitational collapse of a homogeneous perfect fluid [31], some rotating and non-rotating Black Hole solutions [32–34] and phenomenon of particle creation in Rastall cosmology [35]. Another important feature of Rastall gravity is that it can explain the accelerated expansion of the universe also [36]. Moreover, in recent times, many observational constraints were satisfied by Rastall gravity theory, like calculation of the age of the universe and the Hubble parameter from this theory agree well with the observed values [37]. It also provides a better explanation for the presence of the matter-dominated era than GR [38]. Also it is free from entropy and age problems of standard cosmology [39] and can predict gravitational lensing accurately [40, 41]. Another scope of this theory includes the positive possibility of occurrence of traversable wormhole solutions [42]. Further, a work highlighted the use of this theory in the Chaplygin model [43], attempting to combine dark matter and dark energy into a single theory, and then studying the structure formation constraints. Ref. [44, 45] discusses the combined treatment of Rastall gravity and scalar-tensor theory, and formed a new Brans-Dicke-Rastall (BDR) gravity, where PPN [46] constraint was satisfied and it led to an accelerated-decelerated cycle in matter-dominated era of the universe. In other words, Rastall gravity has provided us with a wide range of application scope in various domains. It converges to GR in a weak field regime and thus satisfies the solar system tests along with other constraints satisfied by GR. It is an important feature of this theory that the field equations are obtained directly from the violation condition of energy conservation law and there is no form of Lagrangian associated with the actual theory [22, 26]. This makes Rastall theory different and unique from the other MTGs including  $f(R)$  theories.

The impacts of the cloud of strings on the properties of black holes have been studied in detail in the last a few years for different modified theories. In a recent study, the cloud of strings and the quintessence have been considered together in Lovelock gravity [47]. The magnetic Lovelock black holes have been considered in Ref. [48] in presence of a cloud of strings. The black hole solution in Rastall gravity surrounded by a cloud of strings has been obtained in Ref. [49] for the first time where the authors studied the Quasinormal Modes (QNMs) explicitly. Being motivated by these studies, in this work, we have considered the non-linearly charged black hole solutions surrounded by a cloud of strings for the first time in Rastall gravity. This study will shed light on the impacts of clouds of strings on the properties of the black hole in presence of non-linear charge distributions. To have a clear picture on the scenario, we have considered two types of non-linear charged distribution in the presence of a cloud of strings in Rastall gravity.

The primary focus of our work shall be on the study of the scalar QNMs of Ayón - Beato - García (ABG) black hole [50] and a new black hole in Rastall gravity with a cloud of strings as the surrounding field. QNMs are basically some complex numbers arising out of emissions of GWs from the compact, massive objects that are undergoing perturbations in spacetime [51]. The real part of the QNM signifies the frequency of GW emission from the source, while the imaginary coefficient represents the damping of GW during its propagation. The idea of QNMs was first proposed by Vishveshwara in 1970 [52] and it was confirmed by Press in his work in 1971 [53]. Later, quasinormal eigenfrequency calculations were done by Chandrasekhar and Detweiler in 1975 [54]. These QNMs and eigenfrequency calculations were utilized to test theories of gravity including GR in [55, 56].

Recently, the study of black holes and neutron stars in Rastall gravity has been frequently carried out with the hope of results of notable deviations from GR. One such work was carried out in Ref. [57], where neutron stars were studied in Rastall theory. On the same line, another work was done in Ref. [33], where black holes were studied in Rastall theory. Black holes surrounded by a perfect fluid were also studied in Rastall gravity in the Ref. [32, 58]. Similar study on QNMs of black holes surrounded by quintessence scalar fields in Rastall gravity was done extensively in [59–61]. QNMs of black hole in Rastall gravity have been studied in Ref. [62], where the variation of QNMs with respect to the Rastall parameter  $\lambda$  has been studied for different perturbations using WKB approximation method. The author showed that for  $k\lambda < 0$  there is a rapid damping of QNMs in gravitational, scalar and electromagnetic fields, whereas for  $k\lambda > 0$  the damping occurs slowly. Further, black holes with non-linear electrodynamic sources were studied in Ref.s [63–65]. In this context, more recently QNMs of black holes with different

non-linear electrodynamic sources in Rastall gravity have been studied in detail in [22]. Here it was found that the behaviour of the black holes and their QNMs depend on the considered surrounding field type.

In this work, we study the QNMs of regular black holes surrounded by a cloud of strings together with a non-linear electrodynamic source in Rastall gravity as mentioned above. Here our aim is to investigate any dependency of the quasinormal frequencies with the charge of black holes, the Rastall parameter and the characteristics of the cloud of strings. The work is organized as follows. In Section II, we derive the charged black hole solutions in Rastall gravity surrounded by a cloud of strings. In Section III, behaviour of potential and QNMs of the black hole solutions are studied explicitly. The properties of the Hawking temperature for the black hole solutions are studied in Section IV. Finally, we conclude the work with a brief summary of the results in Section V. Throughout the paper, we have used the natural unit system ( $G = c = 1$ ).

## II. CHARGED BLACK HOLE SOLUTIONS SURROUNDED BY A CLOUD OF STRINGS IN RASTALL GRAVITY

The Rastall gravity is a type of modification of GR in which the general covariant conservation condition  $T^{\mu\nu}_{;\nu} = 0$  is changed to the following form:

$$\nabla_\nu T^{\mu\nu} = \lambda \nabla^\mu R, \quad (1)$$

where  $\lambda$  is known as the Rastall parameter. This condition modifies the general energy momentum conservation in presence of non-vanishing curvature. When the curvature tends to zero, i.e. in absence of any matter energy content the theory tends to GR. The consequent Rastall field equations are given by [22, 26]

$$R_{\mu\nu} - \frac{1}{2} (1 - 2\beta) g_{\mu\nu} R = \kappa T_{\mu\nu}. \quad (2)$$

Taking trace of the above equation, we obtain

$$R = \frac{\kappa}{(4\beta - 1)} T, \quad \beta \neq 1/4, \quad (3)$$

where we have used  $\beta = \kappa\lambda$  and from here onwards we shall denote  $\beta$  as the Rastall parameter. Now, to obtain the black hole solutions in this framework, we consider the following ansatz:

$$ds^2 = f(r)dt^2 - \frac{dr^2}{f(r)} - r^2 d\Omega^2, \quad (4)$$

which represents a spherically symmetric general spacetime metric in Schwarzschild coordinate. Here  $f(r)$  is the metric function and  $d\Omega^2 = d\theta^2 + \sin^2\theta d\phi^2$ . Next, we define the Rastall tensor as  $\mathcal{S}_{\mu\nu} = \mathcal{G}_{\mu\nu} + \beta g_{\mu\nu} R$ , where  $\mathcal{G}_{\mu\nu}$  is the Einstein tensor. The Rastall tensor has the following components:

$$\begin{aligned} \mathcal{S}^0_0 &= \mathcal{G}^0_0 + \beta R = \frac{1}{f(r)} \mathcal{G}_{00} + \beta R = -r^{-2} \left\{ f'(r)r - 1 + f(r) \right\} + \beta R, \\ \mathcal{S}^1_1 &= \mathcal{G}^1_1 + \beta R = -f(r) \mathcal{G}_{11} + \beta R = -r^{-2} \left\{ f'(r)r - 1 + f(r) \right\} + \beta R, \\ \mathcal{S}^2_2 &= \mathcal{G}^2_2 + \beta R = -r^{-2} \mathcal{G}_{22} + \beta R = -r^{-2} \left\{ r f'(r) + \frac{1}{2} r^2 f''(r) \right\} + \beta R, \\ \mathcal{S}^3_3 &= \mathcal{G}^3_3 + \beta R = -\frac{1}{r^2 \sin^2\theta} \mathcal{G}_{33} + \beta R = -r^{-2} \left\{ r f'(r) + \frac{1}{2} r^2 f''(r) \right\} + \beta R, \end{aligned} \quad (5)$$

where the Ricci scalar reads as

$$R = r^{-2} \left\{ r^2 f''(r) + 4r f'(r) - 2 + 2f(r) \right\} \quad (6)$$

and the prime denotes the derivative with respect to the radial coordinate  $r$ . We define a general total energy momentum tensor  $T^\mu_\nu$  as

$$T^\mu_\nu = E^\mu_\nu + \mathcal{T}^\mu_\nu, \quad (7)$$

where  $\mathcal{T}^\mu_\nu$  is the energy-momentum tensor for the surrounding field, which we will define later and  $E^\mu_\nu$  is the trace-free Maxwell tensor expressed as

$$E_{\mu\nu} = \frac{2}{\kappa} \left( F_{\mu\alpha} F_\nu^\alpha - \frac{1}{4} g_{\mu\nu} F^{\alpha\beta} F_{\alpha\beta} \right), \quad (8)$$

where  $F_{\mu\nu}$  is the antisymmetric Faraday tensor, which satisfies the conditions:

$$\begin{aligned} F^{\mu\nu}{}_{;\mu} &= 0, \\ \partial_{[\sigma} F_{\mu\nu]} &= 0, \end{aligned} \quad (9)$$

For spherical symmetry it gives,

$$F^{01} = \frac{q}{r^2}. \quad (10)$$

This parameter  $q$  plays the role of electrostatic charge in the theory. Hence, the Maxwell tensor takes the form:

$$E^{\mu}{}_{\nu} = \frac{q^2}{\kappa r^4} \begin{pmatrix} 1 & 0 & 0 & 0 \\ 0 & 1 & 0 & 0 \\ 0 & 0 & -1 & 0 \\ 0 & 0 & 0 & -1 \end{pmatrix}. \quad (11)$$

In GR, the first static spherically symmetric black hole solution surrounded by a cloud of string was introduced by Letelier [66]. Considering a cloud of strings as world sheets, one can write the energy-momentum tensor of a cloud of strings characterized by a proper density  $\rho_c$  as given by

$$\mathcal{T}^{\mu\nu} = \frac{\rho_c \Sigma^{\mu\beta} \Sigma_{\beta}{}^{\nu}}{\sqrt{-\gamma}}, \quad (12)$$

where  $\gamma = \frac{1}{2} \Sigma^{\mu\nu} \Sigma_{\mu\nu}$ . The string bivector  $\Sigma^{\mu\nu}$  is expressed as

$$\Sigma^{\mu\nu} = \epsilon^{ab} \frac{\partial x^{\mu}}{\partial \xi^a} \frac{\partial x^{\nu}}{\partial \xi^b}, \quad (13)$$

where  $\epsilon^{ab}$  is the two-dimensional Levi-Civita symbol with  $\epsilon^{01} = -\epsilon^{10} = 1$ . Here, one can see that the cloud of strings is spherically symmetric and hence it is a function of the radial coordinate  $r$  only. As a result, one can have the density  $\rho_c$  and the string bivector  $\Sigma^{\mu\nu}$  as functions of the radial coordinate  $r$  only. Thus, the non-zero components of antisymmetric  $\Sigma^{\mu\nu}$  are found to be  $\Sigma^{01}$  and  $\Sigma^{10}$ . They are related as  $\Sigma^{01} = -\Sigma^{10}$ . Hence, the energy-momentum tensor of cloud of strings takes the following form:

$$\mathcal{T}^{\mu}{}_{\nu} = \begin{pmatrix} \rho_c(r) & 0 & 0 & 0 \\ 0 & \rho_c(r) & 0 & 0 \\ 0 & 0 & 0 & 0 \\ 0 & 0 & 0 & 0 \end{pmatrix}. \quad (14)$$

From Eq.s (1), (3) and (14) we may write,

$$\frac{d\rho_c}{dr} + \frac{2\rho_c}{r} = \frac{2\beta}{4\beta - 1} \frac{d\rho_c}{dr}. \quad (15)$$

The solution of the above equation reads,

$$\rho_c(r) = b r^{-\frac{2(4\beta-1)}{2\beta-1}}, \quad (16)$$

where  $b$  is an integration constant. It is associated with the density of the cloud of strings. The weak energy condition demands that  $b \geq 0$ . Now the  $\mathcal{S}^0_0 = T^0_0$  and  $\mathcal{S}^1_1 = T^1_1$  components of Rastall field equations give,

$$-r^{-2} (r f' - 1 + f) + \frac{\beta}{r^2} (r^2 f'' + 4r f' - 2 + 2f) = \kappa \rho_c + \frac{q^2}{r^4}, \quad (17)$$

Similarly, the  $\mathcal{S}^2_2 = T^2_2$  and  $\mathcal{S}^3_3 = T^3_3$  components take the form:

$$-r^{-2} \left( r f' + \frac{1}{2} r^2 f'' \right) + \frac{\beta}{r^2} (r^2 f'' + 4r f' - 2 + 2f) = -\frac{q^2}{r^4}. \quad (18)$$

Solving Eq.s (17) and (18), we get the general solution for the metric function,

$$f(r) = 1 - \frac{2M}{r} + \frac{q^2}{r^2} + \frac{a(2\beta - 1)^2 r^{\frac{4\beta}{1-2\beta}}}{8\beta^2 + 2\beta - 1}, \quad (19)$$

where  $a = \kappa b$ . We shall call this term  $a$  as cloud of string parameter as from (16), one can see that this parameter or the integration constant  $b$  directly accounts for the cloud of string density. This parameter is again restricted by weak energy condition  $a \geq 0$ .

With Eq. (19), the metric (4) takes the form:

$$ds^2 = \left( 1 - \frac{2M}{r} + \frac{q^2}{r^2} + \frac{a(2\beta - 1)^2 r^{\frac{4\beta}{1-2\beta}}}{8\beta^2 + 2\beta - 1} \right) dt^2 - \frac{dr^2}{1 - \frac{2M}{r} + \frac{q^2}{r^2} + \frac{a(2\beta - 1)^2 r^{\frac{4\beta}{1-2\beta}}}{8\beta^2 + 2\beta - 1}} - r^2 d\Omega^2. \quad (20)$$

The above metric (20) represents Reissner-Nordström black hole surrounded by a cloud of strings in Rastall gravity. The Ricci scalar for the above metric is given by

$$R = \frac{2ar^{\frac{4\beta}{1-2\beta}-2}}{4\beta - 1}. \quad (21)$$

One can see from this equation that the Ricci scalar depends on the Rastall parameter  $\beta$  as well as the cloud of string parameter  $a$ , but not the charge of the black hole  $q$ . The Ricci squared is given by

$$R_{\mu\nu}R^{\mu\nu} = 2r^{-8} \left( \frac{a^2 (8\beta^2 - 4\beta + 1) r^{\frac{4}{1-2\beta}}}{(1 - 4\beta)^2} + 2aq^2 r^{\frac{2}{1-2\beta}} + 2q^4 \right), \quad (22)$$

and the Kretschmann scalar is

$$R_{\alpha\beta\mu\nu}R^{\alpha\beta\mu\nu} = 4r^{-8} \left( \frac{a^2 (4\beta(\beta(4\beta(14\beta - 9) + 11) - 2) + 1) r^{\frac{4}{1-2\beta}}}{(8\beta^2 + 2\beta - 1)^2} + \frac{2ar^{\frac{2}{1-2\beta}} (2(1 - 6\beta)Mr + (14\beta - 1)q^2)}{2\beta + 1} + 2(6M^2r^2 - 12Mq^2r + 7q^4) \right). \quad (23)$$

From the expressions (21), (22) and (23), one can see that the black hole is a singular black hole for any values of  $a$  and  $\beta$ . The Kretschmann scalar as well as the Ricci squared depends on the electrodynamic source. In the limit of  $\beta \rightarrow 0$  and  $q \rightarrow 0$  in the metric (20), one can recover the black hole surrounded by a cloud of strings in GR [66] as

$$ds^2 = \left( 1 - \frac{2M}{r} - a \right) dt^2 - \frac{dr^2}{1 - \frac{2M}{r} - a} - r^2 d\Omega^2. \quad (24)$$

One may note that the spacetime represented by this metric (24) is asymptotically flat as the third term  $a$  in the metric function is a constant term. One may realise this from the Ricci curvature from Eq. (6), which gives for this metric as

$$R = -\frac{2a}{r^2}. \quad (25)$$

At asymptotic limit i.e.  $r \rightarrow \infty$ ,

$$R = 0. \quad (26)$$

Which represents flat spacetime for any values of  $a$ . Hence, in GR, the term  $a$  can mimic the deficit angle [67, 68]. However, in Rastall gravity, due to the presence of  $\beta$ , the term can not mimic the deficit angle. Hence, in Rastall gravity,  $a$  is expected to provide different signatures on QNMs depending on the value of  $\beta$ .

The QNMs of non-linearly charged black holes surrounded by dark energy type fields were studied recently in [22]. In this study it was seen that the QNMs of non-linearly charged black holes vary significantly from that of linearly charged black holes. However, till now to the best of our knowledge, no study has been done using non-linearly charged black holes surrounded by a cloud of strings in Rastall gravity. Thus this study will shed some light on the behaviour of black holes in Rastall gravity with non-linear electrodynamic sources and also surrounded by a cloud of strings. In this study, we shall study two types of non-linearly charged black holes viz., ABG black hole and a new black hole in Rastall gravity surrounded by a cloud of strings.

### A. Ayón - Beato - García Black Hole surrounded by a Cloud of Strings

Here we use a non-linear electrodynamic distribution function  $\sigma(r)$  and with this function we can modify the metric (20) as [22]:

$$ds^2 = \left( 1 - \frac{2m(r)}{r} + \frac{a(2\beta - 1)^2 r^{\frac{4\beta}{1-2\beta}}}{8\beta^2 + 2\beta - 1} \right) dt^2 - \frac{dr^2}{1 - \frac{2m(r)}{r} + \frac{a(2\beta - 1)^2 r^{\frac{4\beta}{1-2\beta}}}{8\beta^2 + 2\beta - 1}} - r^2 d\Omega^2, \quad (27)$$

where

$$m(r) = \frac{\sigma(r)}{\sigma_\infty} M.$$

The function  $\sigma(r) > 0$  and  $\sigma'(r) > 0$  for  $r \geq 0$ . Again,  $\sigma(r)/r \rightarrow 0$  as  $r \rightarrow 0$ .  $\sigma_\infty$  is a normalisation constant at infinity, i.e.  $\sigma_\infty = \sigma(r \rightarrow \infty)$ . For the ABG black hole the function  $m(r)$  takes the form [50]:

$$m_{ABG}(r) = M \left\{ 1 - \tanh \left( \frac{q^2}{2Mr} \right) \right\}. \quad (28)$$

Using this ABG function the metric (27) can be written as

$$ds^2 = \left( 1 - \frac{2M \{1 - \tanh(\frac{q^2}{2Mr})\}}{r} + \frac{a(2\beta - 1)^2 r^{\frac{4\beta}{1-2\beta}}}{8\beta^2 + 2\beta - 1} \right) dt^2 - \frac{dr^2}{1 - \frac{2M \{1 - \tanh(\frac{q^2}{2Mr})\}}{r} + \frac{a(2\beta - 1)^2 r^{\frac{4\beta}{1-2\beta}}}{8\beta^2 + 2\beta - 1}} - r^2 d\Omega^2. \quad (29)$$

This is the ABG black hole solution surrounded by a cloud of strings in Rastall gravity. The ABG black hole is a regular black hole [50], which removes the singularity issue arising from the terms containing the mass and charge of the black hole. However, in this case, we expect three black hole horizons due to the mass, charge and surrounding field terms containing the hairs of the black hole. Thus, if we do not have any singularity issue arising from the surrounding field terms, the black hole will be a regular one.

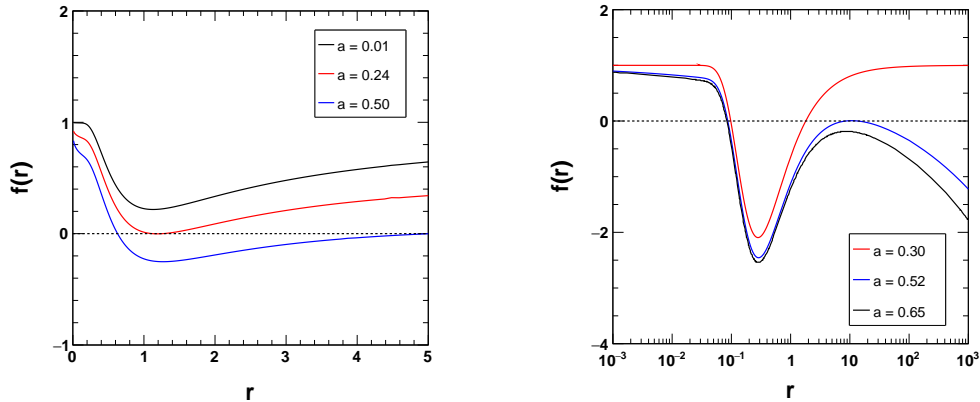


FIG. 1: Variation of the metric function  $f(r)$  with respect to  $r$  for the ABG black hole metric (29) in Rastall gravity surrounded by a cloud of strings with  $q = 1.2$ ,  $\beta = 0.05$  and  $M = 1$  (on left panel), and  $q = 0.6$ ,  $\beta = 0.05$  and  $M = 1$  (on right panel) for different  $a$  values.

To see the properties of this black hole properly, we have plotted the metric function of the black hole with respect to  $r$ . In Fig. 1 the black hole metric  $f(r)$  is plotted with respect to  $r$  taking  $q = 1.2$ ,  $\beta = 0.05$  and  $M = 1$  (on left panel), and  $q = 0.6$ ,  $\beta = 0.05$  and  $M = 1$  (on right panel) for different  $a$  values. One can see that for the plot on the left panel, the critical value of  $a$  is around 0.24. At this value of  $a$ , in the small  $r$  regime, we have one horizon of the black hole. If the value of  $a$  is increased beyond this, two horizons are obtained within the small  $r$  range. Basically, the charge and the mass of the black hole are responsible for the first dip in the curves, but the cloud of strings parameter  $a$  has very small impact on it unless the charge is high. This can be properly visualized from the plot on the right panel of Fig. 1. Here the charge  $q = 0.6$  and the variation of  $a$  imposes very less impact on the first dip of the curves. Thus for small charges, the first horizon of the black hole is affected slightly for different values of  $a$ . However, the second horizon varies significantly with respect to  $a$ . The last horizon or the third horizon which is appearing due to the cloud of strings field has the maximum  $a$  dependency as expected. Hence, we will call

the third horizon as the cloud of string field horizon,  $r_c$ . From the plot on the right panel of this figure, one can also see that for the second and the third horizon the critical value of  $a$  is around 0.52 and above this value, the second and the third horizon disappear completely. Below this critical value three horizons are obtained. But if  $a$  is lowered further, the third horizon moves towards  $+\infty$  and at  $a = 0$  the third horizon vanishes.

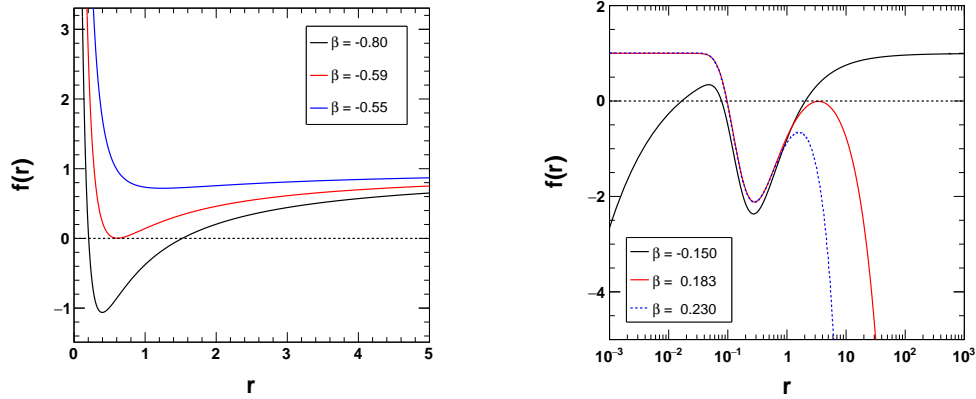


FIG. 2: Variation of the metric function  $f(r)$  with respect to  $r$  for the ABG black hole metric (29) in Rastall gravity surrounded by cloud of strings with  $q = 0.6$ ,  $a = 0.1$  and  $M = 1$  for different  $\beta$  values.

In Fig. 2 the metric function  $f(r)$  is plotted with respect to  $r$  for different values of  $\beta$ . Figure shows that the Rastall parameter  $\beta$  can influence all the three horizons of the black hole. The plot on the left panel shows that for  $\beta$  around  $-0.59$ , we have only one horizon of the black hole. For any values greater than this, naked singularity is formed. For  $\beta$  around 0.183 (see the plot on the right panel of Fig. 2), the black hole has two horizons. In this case, the cloud of string horizon i.e.  $r_c$  and the second horizon coincide to give a single horizon. If one increases  $\beta$  beyond this value, the black hole shows one horizon only. Thus, the Rastall parameter can introduce significant changes on all the horizons of the black hole. Positive values of  $\beta$  influence the cloud of string horizon  $r_c$  most, while the negative  $\beta$  has more impacts on the first and second horizons of the black hole.

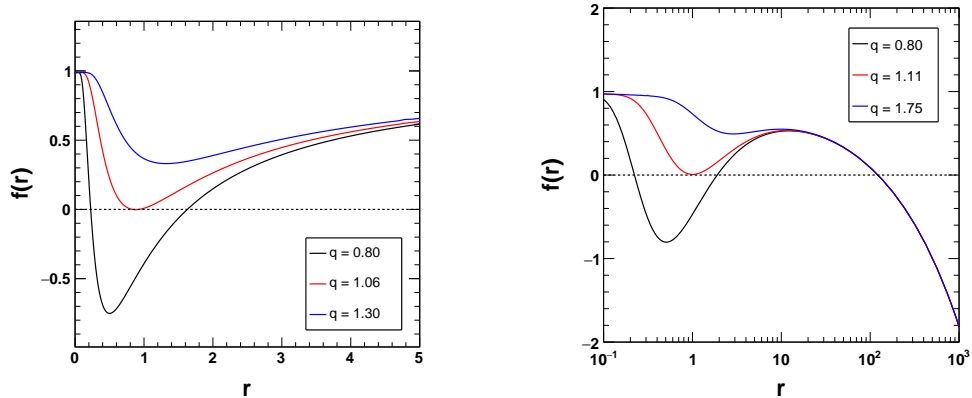


FIG. 3: Variation of metric function  $f(r)$  with respect to  $r$  for ABG black hole metric (29) in Rastall gravity surrounded by a cloud of strings with  $\beta = -0.01$ ,  $a = 0.01$  and  $M = 1$  (on left panel), and  $\beta = 0.1$ ,  $a = 0.1$  and  $M = 1$  (on right panel) for different  $q$  values.

As already seen, another important parameter of the black hole is its charge  $q$ . To clearly see the impact of this parameter on the black hole structure, the plots of the metric function  $f(r)$  with respect to  $r$  for different values of charge  $q$  of the black hole are shown in Fig. 3. Here, for the plot on the left panel we have chosen  $\beta = -0.01$ ,  $a = 0.01$  and  $M = 1$ . We see that for the  $q$  around 1.06, the first and the second horizons combine to give a single horizon. For this set of parameters, the charge  $q > 1.06$  can give naked singularity if there is no cloud of string horizon, i.e.  $r_c$  is present. For the plot on the right panel, we have considered  $\beta = 0.1$ ,  $a = 0.1$  and  $M = 1$ . This plot clearly shows that a variation in charge does not have any significant influences over the cloud of string horizon  $r_c$ . In this case, for the  $q$  around 1.11, we obtain only two black hole horizons and for  $q > 1.11$ , we have only one horizon of the black hole which is the cloud of string horizon  $r_c$ .

It is possible to obtain the expression for the associated electric field from the field equations. In presence of non-linear

electrodynamic sources, the effective energy momentum tensor can be written as

$$T_{\mu\nu} = L(F)g_{\mu\nu} - L_F F_{\mu\lambda} F_{\nu}^{\lambda} + \mathcal{T}_{\mu\nu}, \quad (30)$$

where  $F = \frac{1}{4} F^{\mu\nu} F_{\mu\nu}$  (Lorentz invariant) and  $L_F = \frac{dL}{dF}$ . Restricting the electric field by considering  $F_{\mu\nu} = E(r)(\delta_{\mu}^0 \delta_{\nu}^1 - \delta_{\mu}^1 \delta_{\nu}^0)$ , we can express the field equations as

$$\begin{aligned} \mathcal{S}^0_0 &= \mathcal{G}^0_0 + \beta R = \frac{1}{f(r)} \mathcal{G}_{00} + \beta R = -r^{-2} \left\{ f'(r)r - 1 + f(r) \right\} + \beta R = -\kappa \left[ L(F) + E^2 L_F - \rho_c(r) \right], \\ \mathcal{S}^1_1 &= \mathcal{G}^1_1 + \beta R = -f(r) \mathcal{G}_{11} + \beta R = -r^{-2} \left\{ f'(r)r - 1 + f(r) \right\} + \beta R = -\kappa \left[ L(F) + E^2 L_F - \rho_c(r) \right], \\ \mathcal{S}^2_2 &= \mathcal{G}^2_2 + \beta R = -r^{-2} \mathcal{G}_{22} + \beta R = -r^{-2} \left\{ r f'(r) + \frac{1}{2} r^2 f''(r) \right\} + \beta R = -\kappa L(F), \\ \mathcal{S}^3_3 &= \mathcal{G}^3_3 + \beta R = -\frac{1}{r^2 \sin^2 \theta} \mathcal{G}_{33} + \beta R = -r^{-2} \left\{ r f'(r) + \frac{1}{2} r^2 f''(r) \right\} + \beta R = -\kappa L(F). \end{aligned} \quad (31)$$

Again the electromagnetic field equations,  $\nabla_{\mu}(F^{\mu\nu} L_F) = 0$  give,

$$E(r) L_F = -\frac{q}{4\pi r^2}. \quad (32)$$

Using the above result in the field Eq.s (31), we can have

$$E(r) = \frac{q \left( 4Mr - q^2 \tanh\left(\frac{q^2}{2Mr}\right) \right) \operatorname{sech}^2\left(\frac{q^2}{2Mr}\right)}{4Mr^3}, \quad (33)$$

which is the expression of the electric field for the ABG type non-linear charge distribution. It is clear from the above expression that the electric field is regular everywhere and asymptotically it results,

$$E(r) \approx \frac{q}{r^2}. \quad (34)$$

This result ascertains that the ABG type black hole becomes a Reissner-Nordström black hole in the asymptotic regime or for a very very small magnitude of charge. Using Eq.s (33) and (32) in the first field equation of Eq.s (31) we can obtain an explicit the form of  $L(F)$  as,

$$L(F) = \frac{q^2 \operatorname{sech}^2\left(\frac{q^2}{2Mr}\right) \left( (2\beta - 1)q^2 \tanh\left(\frac{q^2}{2Mr}\right) + 2Mr \right)}{16\pi M r^5}. \quad (35)$$

It may be noted that one may also obtain this expression directly from third or fourth field equation of Eq.s (31).

Now to see the black hole nature, we calculate Ricci scalar, Ricci squared and Kretschmann scalar. These scalars are helpful to predict the singularity of the black hole, if there exists any. Ricci scalar for ABG black hole is

$$R = \frac{2ar^{\frac{4\beta}{1-2\beta}-2}}{4\beta-1} - \frac{8q^4 \sinh^4\left(\frac{q^2}{2Mr}\right) \operatorname{csch}^3\left(\frac{q^2}{Mr}\right)}{Mr^5}. \quad (36)$$

Ricci squared is found to be,

$$R_{\mu\nu} R^{\mu\nu} = \frac{4M(2\beta M + M) \left( a(1-2\beta)r^{\frac{-2}{1-2\beta}} + (1-4\beta)q^2 \operatorname{sech}^2\left(\frac{q^2}{2Mr}\right) \right)^2 + X}{2(1-4\beta)^2 M r^8 (2\beta M + M)} \quad (37)$$

where,

$$X = (2\beta + 1) r^{-2} \left( (4\beta - 1)q^2 \left( q^2 \tanh\left(\frac{q^2}{2Mr}\right) - 2Mr \right) \operatorname{sech}^2\left(\frac{q^2}{2Mr}\right) - 4a\beta M r^{\frac{4\beta}{1-2\beta}+3} \right)^2.$$

And finally the Kretschmann scalar is

$$R_{\alpha\beta\mu\nu} R^{\alpha\beta\mu\nu} = 4r^{-10} \left( r^6 \left( \frac{a(1-2\beta)^2 r^{\frac{4\beta}{1-2\beta}}}{8\beta^2 + 2\beta - 1} + \frac{2M \left( \tanh\left(\frac{q^2}{2Mr}\right) - 1 \right)}{r} \right)^2 + r^2 Y^2 \right) \quad (38)$$



where,

$$Y = y_1^2 + 4 \left( \frac{a\beta(6\beta - 1)r^{\frac{4\beta}{1-2\beta}+3}}{8\beta^2 + 2\beta - 1} + Mr^2 y_2 + q^2 r \operatorname{sech}^2 \left( \frac{q^2}{2Mr} \right) - \frac{2q^4 \sinh^4 \left( \frac{q^2}{2Mr} \right) \operatorname{csch}^3 \left( \frac{q^2}{Mr} \right)}{M} \right),$$

$$y_1 = \frac{4a\beta(2\beta - 1)r^{\frac{2}{1-2\beta}}}{8\beta^2 + 2\beta - 1} + 2Mr y_2 + q^2 \operatorname{sech}^2 \left( \frac{q^2}{2Mr} \right),$$

$$y_2 = \left( \tanh \left( \frac{q^2}{2Mr} \right) - 1 \right).$$

From the above expressions it is seen that the Ricci scalar for this black hole differs completely from the Ricci scalar of Reissner-Nordström black hole. In case of the Reissner-Nordström black hole surrounded by a cloud of strings in Rastall gravity defined by the metric (20), the Ricci scalar is independent of the charge of the black hole. But in this case, Ricci scalar depends on the charge of the black apart from the Rastall parameter. Thus, the non-linear charge distribution function used in Eq. (30) has a significant impact over the Ricci scalar of the ABG black hole. The Ricci squared and the Kretschmann scalar are also different from the Reissner-Nordström black hole surrounded by a cloud of strings in Rastall gravity. However, one important point worth to mention is that for this case, at  $\beta = 0$ , i.e. at the GR limit, we have a regular black hole. In case of Rastall gravity, we see that for  $0.25 < \beta < 0.50$ , the singularity issue arising from the terms containing  $\beta$  vanish resulting in a regular black hole. This constraint on  $\beta$  can be obtained from the Kretschmann scalar (38). It is seen from Eq. (38) that for the Kretschmann scalar to be finite at the limit  $r \rightarrow 0$ , the  $\beta$  dependent terms should not diverge. One may note that due to the consideration of the ABG non-linear charge distribution, one does not get singularity issues from the mass and charge dependent terms in the metric and the scalars. Now, taking account of the mass and charge independent terms in the Eq. (38), we have obtained that  $0.25 < \beta < 0.50$  gives a regular black hole solution.

### B. A new Black Hole solution surrounded by a Cloud of Strings

At this stage as a possible alternative to the function (28), we introduce a new distribution function as given by

$$m(r) = M \left\{ 1 + \operatorname{arcCsch} \left( \zeta - \frac{2Mr}{q^2} \right) \right\}, \quad (39)$$

for which the black hole metric (27) can be expressed as

$$ds^2 = \left( 1 - \frac{2M \{ 1 + \operatorname{arcCsch}(\zeta - \frac{2Mr}{q^2}) \}}{r} + \frac{a(2\beta - 1)^2 r^{\frac{4\beta}{1-2\beta}}}{8\beta^2 + 2\beta - 1} \right) dt^2 - \frac{dr^2}{1 - \frac{2M \{ 1 + \operatorname{arcCsch}(\zeta - \frac{2Mr}{q^2}) \}}{r} + \frac{a(2\beta - 1)^2 r^{\frac{4\beta}{1-2\beta}}}{8\beta^2 + 2\beta - 1}} - r^2 d\Omega^2. \quad (40)$$

Here  $\zeta$  is a free model parameter. To study the behaviour of this metric of the black hole, we have plotted the metric function  $f(r)$  with respect to  $r$  for different values of  $a$  in Fig. 4. On the left panel of Fig. 4, we have chosen  $q = 1.15$ ,  $\beta = 0.1$ ,  $\zeta = -0.05$  and  $M = 1$ . For this case, we show that when the value of  $a$  is around 0.19, the first and second horizons of the black hole are coincided to give a single horizon and for  $a < 0.19$ , only the third horizon  $r_c$  is left. For the plot on the right panel, we have considered  $q = 0.6$ ,  $\beta = 0.05$ ,  $\zeta = -0.8$  and  $M = 1$ . In this case, we see that variation of  $a$  has comparatively less influence over the first horizon and for  $a$  around 0.54, the second and the third horizons are combined to give a single horizon. For this set of parameters, if one increases  $a$  beyond 0.54, the second and the third horizon of the black hole vanish completely.

In Fig. 5 the metric function  $f(r)$  is plotted with respect to  $r$  for different  $\beta$  values. Similar to the previous black hole metric, here also we have seen that the Rastall parameter  $\beta$  can influence all the three horizons of the black hole. For the plot on the left panel of this figure it is seen that for  $\beta$  around  $-0.808$  the first and second horizons are combined to a single horizon. For  $\beta > -0.808$ , first and second horizons vanish and there can be a naked horizon for small values of  $a$ . While on the right panel one can see that for the  $\beta$  around 0.10, the second and third horizons are coincided to result in a single black hole horizon. For  $\beta > 0.10$ , second and third horizons vanish completely.

Similarly, the  $f(r)$  function is plotted with respect to  $r$  for different values of the charge  $q$  in Fig. 6. Here, on the left panel we have used  $\beta = 0.1$ ,  $a = 0.01$ ,  $\zeta = 0.4$  and  $M = 1$ , and on the right panel  $\beta = 0.1$ ,  $a = 0.1$ ,  $\zeta = -0.8$  and  $M = 1$  are

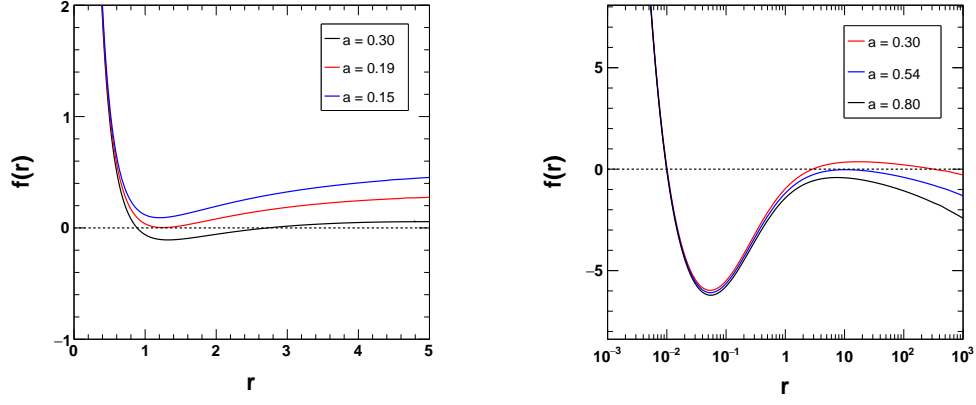


FIG. 4: Variation of metric function  $f(r)$  with respect to  $r$  for the black hole defined by metric (40) with  $q = 1.15$ ,  $\beta = 0.1$ ,  $\zeta = -0.05$  and  $M = 1$  (on left panel), and  $q = 0.60$ ,  $\beta = 0.05$ ,  $\zeta = -0.80$  and  $M = 1$  (on right panel) for different  $a$  values.

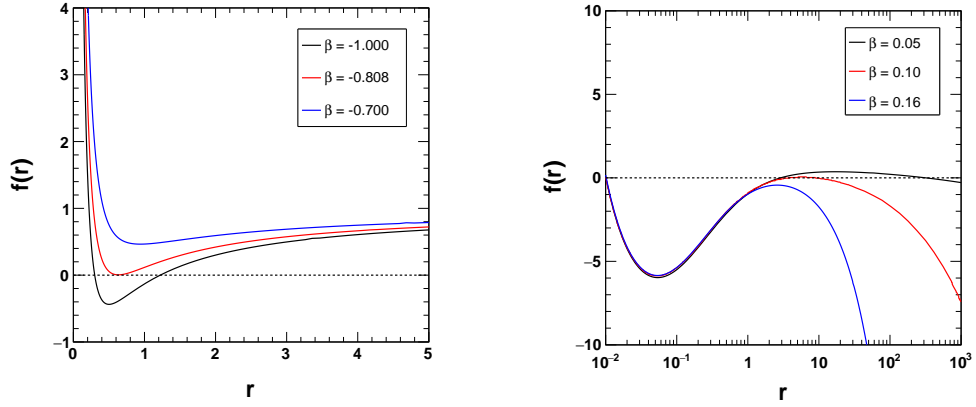


FIG. 5: Variation of metric function  $f(r)$  with respect to  $r$  for the black hole defined by metric (40) with  $q = 0.6$ ,  $a = 0.3$ ,  $\zeta = -0.5$  and  $M = 1$  (on left panel), and  $q = 0.6$ ,  $a = 0.3$ ,  $\zeta = -0.8$  and  $M = 1$  (on right panel) for different  $\beta$  values.

used. In both cases, we see that charge  $q$  has negligible effect on the third horizon, i.e. the cloud of string horizon  $r_c$ . On the left panel, for  $q$  around 0.953, first and second horizons are combined to give a single horizon and for  $q > 0.953$ , first and the second horizons vanish completely. On the right panel,  $q > 1.62$  values give a single horizon ( $r_c$ ) of the black hole.

Finally, in Fig. 7 we have plotted the metric function with respect to  $r$  for different values of the model parameter  $\zeta$ . We see that the impact of  $\zeta$  on the metric function is similar to the charge  $q$ . On the left panel of this figure, we have used  $\beta = 0.1$ ,  $a = 0.05$ ,  $q = 1$  and  $M = 1$ . We see that for  $\zeta = 0.2$  ( $\zeta_c$ , the critical value), first and the second horizons of the black hole are coincided and for any other values greater than this, first and second horizons of the black hole vanish completely. On the right panel of the figure, we have increased  $a$  to 0.1 and decreased  $q$  slightly to 0.8. We observe that increase in the value of  $a$ , increases the critical value  $\zeta_c$ . For this case, it is  $\zeta_c = 1.90$  and for any other  $\zeta > \zeta_c$ , first and the second horizons vanish completely.

For the black hole metric (40), the expression for associated electric field is given by

$$E(r) = \frac{2M^2q(16M^3r^3 - 20\zeta M^2q^2r^2 + (8\zeta^2 + 3)Mq^4r - \zeta(\zeta^2 + 1)q^6)}{(2Mr - \zeta q^2)^3 \sqrt{\frac{1}{(\zeta - \frac{2Mr}{q^2})^2} + 1} (4M^2r^2 - 4\zeta Mq^2r + (\zeta^2 + 1)q^4)}. \quad (41)$$

This expression shows that  $\zeta$  has significant contributions to the electric field associated with the black hole. The electric field is regular everywhere and similar to the previous case, asymptotically it gives,

$$E(r) \approx \frac{q}{r^2}. \quad (42)$$

So, although the functional form is different, the charge distributions are equivalent in the asymptotic region. Both the black holes, therefore, can give Reissner-Nordström black hole in the limiting situation  $q \rightarrow 0$ , i.e. for very small charge. To have a

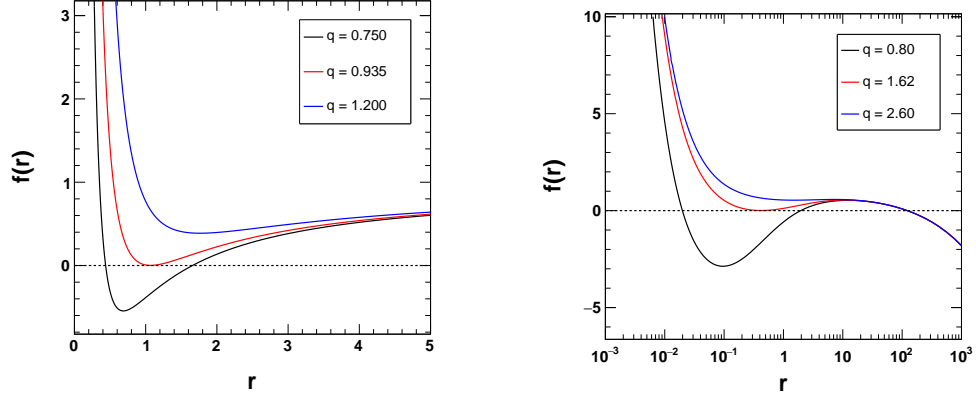


FIG. 6: Variation of metric function  $f(r)$  with respect to  $r$  for the black hole defined by metric (40) with  $\beta = 0.1$ ,  $a = 0.01$ ,  $\zeta = 0.4$  and  $M = 1$  (on left panel), and  $\beta = 0.1$ ,  $a = 0.1$ ,  $\zeta = -0.8$  and  $M = 1$  (on right panel) for different  $q$  values.

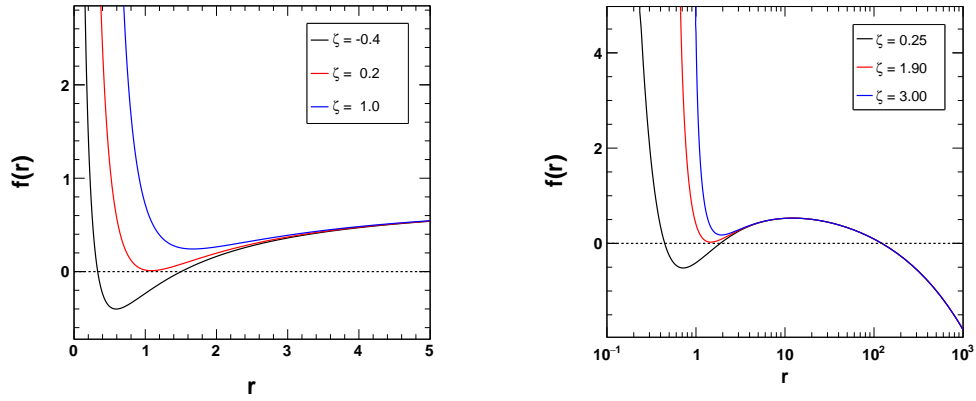


FIG. 7: Variation of metric function  $f(r)$  with respect to  $r$  for the black hole defined by metric (40) with  $\beta = 0.1$ ,  $a = 0.05$ ,  $q = 1$  and  $M = 1$  (on left panel), and  $\beta = 0.1$ ,  $a = 0.1$ ,  $q = 0.8$  and  $M = 1$  (on right panel) for different  $\zeta$  values.

better view on the regularity of the black hole, we calculate Ricci scalar, Ricci squared and Kretschmann scalar for this black hole. Ricci scalar for this black hole metric (40) is

$$R = 8r^{-2} \left( \frac{ar^{\frac{4\beta}{1-2\beta}}}{16\beta - 4} + \frac{M^2q^4 (4\zeta M^2r^2 - (4\zeta^2 + 1)Mq^2r + \zeta(\zeta^2 + 1)q^4) \sqrt{\frac{q^4}{(\zeta q^2 - 2Mr)^2} + 1}}{(2Mr - \zeta q^2)(4M^2r^2 - 4\zeta Mq^2r + (\zeta^2 + 1)q^4)^2} \right). \quad (43)$$

The Ricci squared is found as

$$R_{\mu\nu}R^{\mu\nu} = Z_5^{-1} \left[ Z_1 Z_2^2 + 2(2 - 8\beta)^2 r^2 Z_4^2 + 8(1 - 4\beta)^2 Z_6^2 \right], \quad (44)$$

where

$$Z_1 = (2 - 8\beta)^2 (\zeta q^2 - 2Mr)^2 Z_3^2,$$

$$Z_2 = a(1 - 2\beta)r^{\frac{4\beta}{1-2\beta}} (4M^2r^2 - 4\zeta Mq^2r + (\zeta^2 + 1)q^4) + 4(1 - 4\beta)M^2q^2 \sqrt{\frac{1}{\left(\zeta - \frac{2Mr}{q^2}\right)^2} + 1},$$

$$Z_3 = (4M^2r^2 - 4\zeta Mq^2r + (\zeta^2 + 1)q^4),$$

$$Z_4 = \left( a\beta r^{\frac{2}{1-2\beta}-3} (2Mr - \zeta q^2) Z_3^2 + Z_7 \right),$$

$$Z_5 = 2(1 - 4\beta)^4 r^4 (\zeta q^2 - 2Mr)^2 Z_3^4,$$

$$Z_6 = \left( a\beta r^{\frac{4\beta}{1-2\beta}} (2Mr - \zeta q^2) Z_3^2 + r Z_7 \right)$$

and

$$Z_7 = 2(4\beta - 1)M^3 q^2 (8M^2 r^2 - 8\zeta M q^2 r + (2\zeta^2 + 1) q^4) \sqrt{\frac{1}{\left(\zeta - \frac{2Mr}{q^2}\right)^2 + 1}}.$$

The Kretschmann scalar is

$$R_{\alpha\beta\mu\nu}R^{\alpha\beta\mu\nu} = 4r^{-6} \left[ 4A^2 + 4(B + C + D)^2 + \left\{ \frac{a(1 - 2\beta)^2 r^{\frac{4\beta}{1-2\beta}+1}}{8\beta^2 + 2\beta - 1} + 2M \left( \operatorname{csch}^{-1} \left( \frac{2Mr}{q^2} - \zeta \right) - 1 \right) \right\}^2 \right], \quad (45)$$

where

$$A = \frac{2a\beta(2\beta - 1)r^{\frac{4\beta}{1-2\beta}+1}}{8\beta^2 + 2\beta - 1} + D,$$

$$B = \frac{a\beta(6\beta - 1)r^{\frac{4\beta}{1-2\beta}+1}}{8\beta^2 + 2\beta - 1},$$

$$C = \frac{4M^3 q^2 r^2}{(2Mr - \zeta q^2)^3 \sqrt{\frac{1}{\left(\zeta - \frac{2Mr}{q^2}\right)^2 + 1}}} + \frac{2M^3 r^2}{q^4 \left(\zeta - \frac{2Mr}{q^2}\right)^5 \left(\frac{1}{\left(\zeta - \frac{2Mr}{q^2}\right)^2 + 1}\right)^{3/2}}$$

and

$$D = \frac{2M^2 q^2 r}{(\zeta q^2 - 2Mr)^2 \sqrt{\frac{1}{\left(\zeta - \frac{2Mr}{q^2}\right)^2 + 1}}} + M \operatorname{csch}^{-1} \left( \frac{2Mr}{q^2} - \zeta \right) - M.$$

From the above expressions it is clear that the Ricci scalar, Ricci square and the Kretschmann scalar depend on the charge  $q$  of the black hole, model parameter  $\zeta$  and the Rastall parameter  $\beta$ . One can see that for  $\zeta = \operatorname{arcCsch}(1) = 0.881374$  and  $0.25 < \beta < 0.50$ , the black hole is a regular one. But for  $\zeta \neq \operatorname{arcCsch}(1)$ , the black hole is singular one. Hence, the metric (40) can represent both regular and singular black holes. However, the regular black hole represented by this metric is not identical to the ABG black hole represented by the metric (29).

### III. QUASINORMAL MODES OF CHARGED BLACK HOLES SURROUNDED BY A CLOUD OF STRINGS

In this section, we shall compute the QNMs for scalar perturbation in case of the black holes defined earlier. To obtain QNMs for the black holes, we shall implement the higher order WKB approximation method which uses higher order derivatives of the black hole potential associated with scalar perturbation in tortoise coordinates. To obtain the expression for the associated black holes' potentials, at first we perturb the black hole with some probe coupled to a scalar field minimally, with the equation of motion,

$$\frac{1}{\sqrt{-g}} \partial_\alpha (\sqrt{-g} g^{\alpha\beta} \partial_\beta) \Phi = \mu^2 \Phi. \quad (46)$$

In this equation  $\mu$  is the mass of the associated scalar field and it is possible to express  $\Phi$  as

$$\Phi(t, r, \theta, \phi) = e^{-i\omega t} \frac{\psi(r)}{r} Y_l^m(\theta, \phi), \quad (47)$$

where  $\psi(r)$  is the radial part and  $Y_l^m(\theta, \phi)$  is the well known spherical harmonics. Using Eq. (47) we can transform Eq. (46) into a Schrödinger like equation, given by

$$\frac{d^2\psi}{dx^2} + (\omega^2 - V(x))\psi = 0, \quad (48)$$

where  $x$  is defined as

$$x = \int \frac{dr}{f(r)}, \quad (49)$$

which is known as the tortoise coordinate. In Eq. (48), the effective potential is given by

$$V(r) = f(r) \left\{ \frac{f'(r)}{r} + \frac{l(l+1)}{r^2} + \mu^2 \right\}. \quad (50)$$

To have a physically consistent system we need to consider boundary conditions to Eq. (48) both at the horizon of the black hole and infinity. For an asymptotically flat spacetime, the quasinormal conditions can be given by [52, 69],

$$\psi(x) \rightarrow \begin{cases} Ae^{+i\omega x} & \text{if } x \rightarrow -\infty \\ Be^{-i\omega x} & \text{if } x \rightarrow +\infty \end{cases}, \quad (51)$$

where  $A$  and  $B$  are the amplitudes of the wave. One can see that the purely ingoing wave physically implies that nothing can escape from the horizon of the black hole. On the other hand, the purely outgoing wave implies that no radiation comes from the infinity. These two expressions can effectively give the quasinormal requirement or condition which ensures existence of infinite set of discrete complex numbers, known as QNMs. For a normal Schwarzschild black hole, the QNMs basically depends on the mass  $M$ , overtone  $n$  and multipole number  $l$  only.

Before going to the QNMs of the black holes, we have compared the potentials associated with both of the black holes. In Fig. 8, we have plotted the potential  $V(r)$  versus  $r$  for different values of multipole number  $l$ . The plot on the left panel shows the variation of the potential  $V(r)$  with respect to  $r$  for the ABG black hole and the plot on the right panel is for the metric (40). One can see that the pattern of variation of both the potentials is identical, but the maximum value of the potential for the ABG black hole is slightly greater than that of the other black hole given by the metric (40). However, this difference is significant only for higher values of the charge  $q$  and for small values of the charge  $q$ , potentials of both the black holes are almost identical. This is due to the fact that the charge distribution functions of both the black holes behave identically in the asymptotic regime.

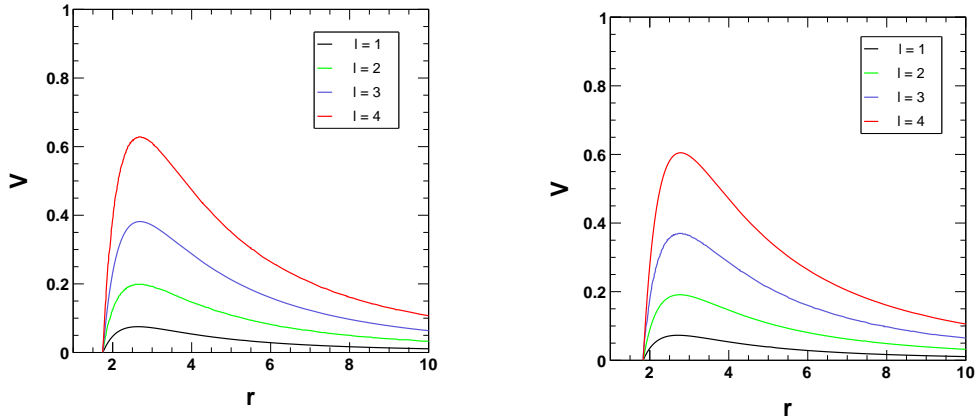


FIG. 8: Potential  $V(r)$  versus  $r$  for the ABG black hole (on left) and for the black hole defined by the metric (40) (on right) with  $a = 0.1$ ,  $\beta = 0.1$ ,  $M = 1$ ,  $q = 0.9$  and  $\zeta = -0.6$ .

The potential  $V(r)$  versus  $r$  is plotted for different values of  $q$  in Fig. 9. Here, we have chosen  $a = 0.1$ ,  $\beta = 0.1$ ,  $M = 1$ ,  $l = 4$  and  $\zeta = -0.6$ . We see that in case of higher values of  $q$ , the maximum value of  $V(r)$  i.e.  $V_{max}$  for the ABG black hole

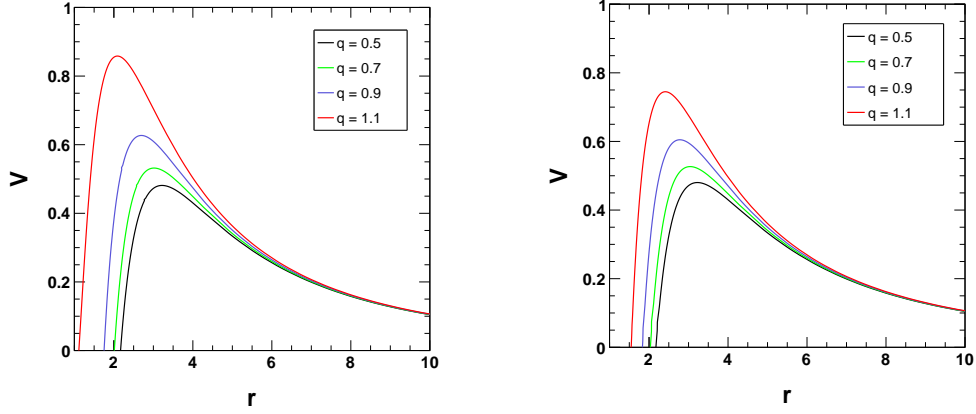


FIG. 9: Potential  $V(r)$  versus  $r$  for the ABG black hole (on left) and for the black hole defined by the metric (40) (on right) with  $a = 0.1$ ,  $\beta = 0.1$ ,  $M = 1$ ,  $l = 4$  and  $\zeta = -0.6$ .

(on left panel) is greater than the other black hole (on the right panel). Apart from this, value of  $r$  corresponding to  $V_{max}$  for the ABG black hole is smaller than the other black hole. However, this change is negligible for small values of the charge  $q$ .

We have shown the variation of potential  $V(r)$  with respect to  $r$  for both of the black holes in Fig. 10 for different values of cloud of string parameter  $a$ . It is seen from the figure that for higher values of  $a$ , potential  $V(r)$  decreases following the same trend for both of the black holes. But for the ABG black hole, the potential is slightly higher than that of the other black hole given by the metric (40). This is again depends on the magnitude of the charge  $q$  as seen from the previous results. For small magnitudes of charge  $q$ , the deviation is very very small.

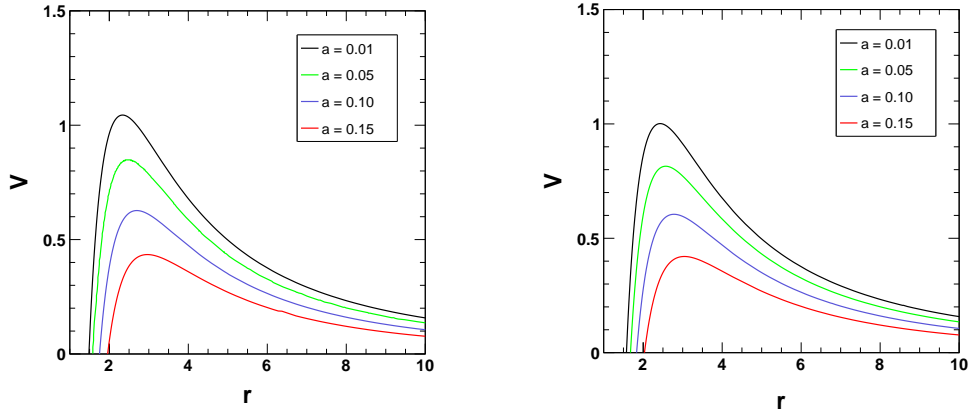


FIG. 10: Variation of potential  $V(r)$  with respect to  $r$  for the ABG black hole (on left) and for the black hole defined by the metric (40) (on right) with  $l = 4$ ,  $\beta = 0.1$ ,  $M = 1$ ,  $q = 0.9$  and  $\zeta = -0.6$ .

The dependency of the potential  $V(r)$  with the Rastall parameter  $\beta$  is shown in Fig. 11 for ABG black hole (on left panel) and for the black hole defined by the metric (40) (on right panel). It is seen that for both the black holes, for  $\beta = -0.10$ , the potential has higher value. The GR limit corresponding to  $\beta = 0$ , gives slightly lower value of the potential and for  $\beta > 0$  potential decreases accordingly. Similarly, for  $\beta = -0.35$  the potential again decreases for both cases, especially for the smaller  $r$  values.

Another important parameter in the black hole represented by the metric (40) is  $\zeta$ . We have plotted the potential corresponding to this black hole in Fig. 12 for different values of  $\zeta$ . It is observed that the parameter has very small impact on the potential for the small charges. However, if we increase the charge  $q$  significantly, we observe noticeable changes in the pattern of the potential as shown in the figure. Here, we have used  $q = 1.2$  in order to see the impacts of  $\zeta$  on the potential significantly. It is clearly seen from the figure that higher positive values of  $\zeta$  increases the potential near small  $r$  values significantly. However, at far distance away from the black hole, the parameter  $\zeta$  has no significant contributions. These impacts of  $\zeta$  on both the metric and potential of the black hole suggest that the nature of this parameter is slightly similar to that of the charge  $q$  of the black hole.

The behaviour of the potential influences the QNMs significantly. From the above study of potentials associated with the

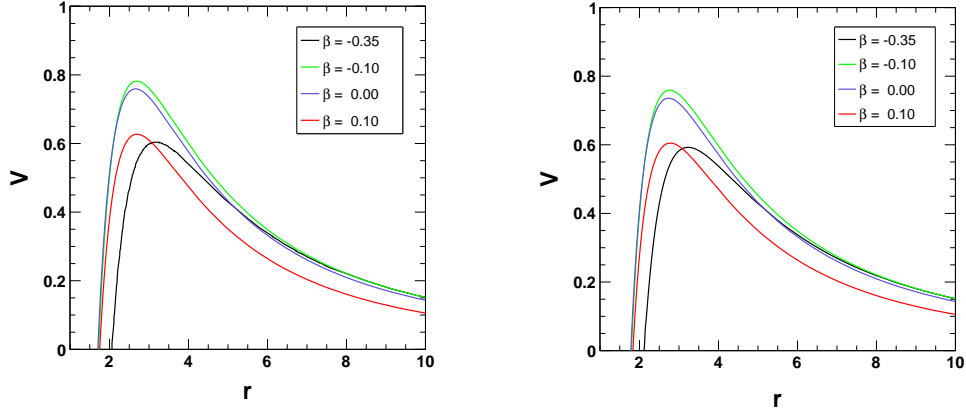


FIG. 11: Behaviour of  $V(r)$  with respect to  $r$  for the ABG black hole (on left) and for the black hole defined by the metric (40) (on right) with  $a = 0.1$ ,  $l = 4$ ,  $M = 1$ ,  $q = 0.9$  and  $\zeta = -0.6$ .

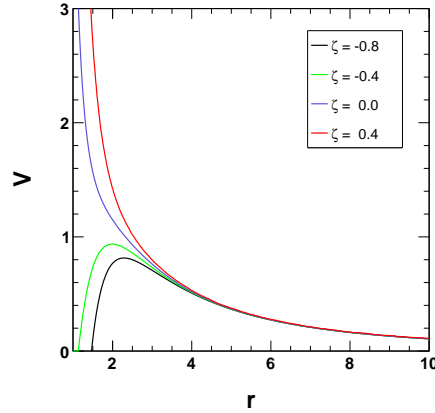


FIG. 12: Behaviour of the potential  $V(r)$  with respect to  $r$  for the different values of the parameter  $\zeta$  of the the black hole defined by the metric (40) with  $a = 0.1$ ,  $\beta = 0.1$ ,  $M = 1$ ,  $q = 1.2$  and  $l = 4$ .

black holes, we see that the black holes differ at higher magnitude of charges and asymptotically they behave identically. In this study of QNMs, we consider a massless scalar field with  $\mu = 0$ . To calculate the QNMs for these black holes, we have used 5th order WKB approximation method [70, 71] as in case of 6th order WKB approximation method, the errors associated with QNMs are comparatively higher. In the WKB approximation method, higher order approximations may not always give higher accuracy and in this case the non-linear charge distribution function also plays a crucial role [22, 71]. QNMs for both the black holes with different  $n$  and  $l$  values are shown in Table I. In this table we have calculated a quantity  $\Delta_k$  defined by [71]

$$\Delta_k = \left| \frac{\omega_{k+1} - \omega_{k-1}}{2} \right|,$$

where  $k$  denotes the order of WKB approximation.  $\Delta_k$  gives a good measurement of the error order [71] in QNMs. In this study, we have used the expression of  $\Delta_k$  to calculate the error  $\Delta_5$  associated with the 5th order WKB approximation for both of the black holes. Moreover, the table contains the  $n < l$  cases only. It is because in WKB approximation method one can't have QNMs for  $n \geq l$  with a satisfactory accuracy [71]. It was also observed that with an increase in  $(l - n)$  value higher accuracy can be obtained in the associated QNMs [22]. From Table I, one can see that for the chosen value of  $\zeta$ , the real quasinormal frequency for the black hole defined by metric (40) i.e. for the second black hole is lower than that for the ABG black hole or the first black hole. The magnitude of imaginary quasinormal frequency is comparatively higher for the second black hole. This suggests that the damping associated with the QNMs of the second black hole is higher. The absolute difference between the QNMs of the black holes increases with increase in  $(l - n)$  values. Another observation from the table is that the errors associated the 5th order WKB approximation are much smaller for the second black hole than that for first one and also higher  $(l - n)$  value gives comparatively higher accuracy in the WKB approximation for both the black holes. To have a better visualization of the variation of QNMs for both the black holes with respect to the black hole model parameters, we have plotted the real and

imaginary quasinormal frequencies of the black holes.

TABLE I: QNMs of the ABG black hole and the other black hole defined by metric (40) (BH02) for  $a = 0.1$ ,  $\beta = 0.1$ ,  $q = 0.7$  and  $\zeta = -0.8$  obtained using the 5th order WKB approximation method.

$n$	$l$	ABG	$\Delta_5(\text{ABG})$	BH02	$\Delta_5(\text{BH02})$	ABG-BH02
$n = 0$	$l = 1$	$0.240478 - 0.0695003i$	0.174093	$0.238837 - 0.0698842i$	0.0000737562	0.0016856
	$l = 2$	$0.40208 - 0.068745i$	0.00185342	$0.399421 - 0.069109i$	0.0000115004	0.00268394
	$l = 3$	$0.563475 - 0.0685916i$	0.00132465	$0.559769 - 0.068895i$	$2.94799 \times 10^{-6}$	0.00371822
	$l = 4$	$0.724769 - 0.0685155i$	0.00210424	$0.720018 - 0.0688071i$	$1.06331 \times 10^{-6}$	0.00475931
	$l = 5$	$0.886016 - 0.0684734i$	0.0000182862	$0.880219 - 0.0687625i$	$4.72176 \times 10^{-7}$	0.00580376
$n = 1$	$l = 2$	$0.390301 - 0.208608i$	0.0233237	$0.387631 - 0.21019i$	0.0000447605	0.00310411
	$l = 3$	$0.55497 - 0.207148i$	0.0162886	$0.551067 - 0.208172i$	0.0000123964	0.0040349
	$l = 4$	$0.718092 - 0.20642i$	0.0274191	$0.713161 - 0.207326i$	$4.62062 \times 10^{-6}$	0.00501355
	$l = 5$	$0.88052 - 0.206017i$	0.000242116	$0.874572 - 0.206895i$	$2.08662 \times 10^{-6}$	0.00601286
$n = 2$	$l = 3$	$0.538845 - 0.349602i$	0.0931067	$0.53476 - 0.351735i$	0.000160981	0.00460834
	$l = 4$	$0.705234 - 0.346878i$	0.17811	$0.699966 - 0.3485i$	0.0000614924	0.00551146
	$l = 5$	$0.869821 - 0.345336i$	0.00156762	$0.863563 - 0.346825i$	0.0000281748	0.00643289

In Fig. 13 we have plotted real QNMs with respect to the cloud of strings parameter  $a$  for the ABG black hole and the black hole defined by the metric (40) with  $q = 0.5$ ,  $M = 1$ ,  $\zeta = -0.4$  and  $\beta = 0.1$  (on left panel), and  $\beta = -0.1$  (on right panel). We can see that for the charge  $q = 0.5$ , QNMs for both the black holes are very close to each other. However, the difference is expected to be more for higher values of the charge  $q$  from the previous study of the black holes. For both the black holes, real quasinormal frequencies,  $\omega_R$  decrease with increase in  $a$  identically. But for  $\beta = -0.1$ , the frequencies decrease slowly in comparison to  $\beta = 0.1$  case, where for  $a = 0.1$ ,  $\omega_R$  decreases below 0.7. This suggests that  $\beta$  might have some significant impacts over the QNMs.

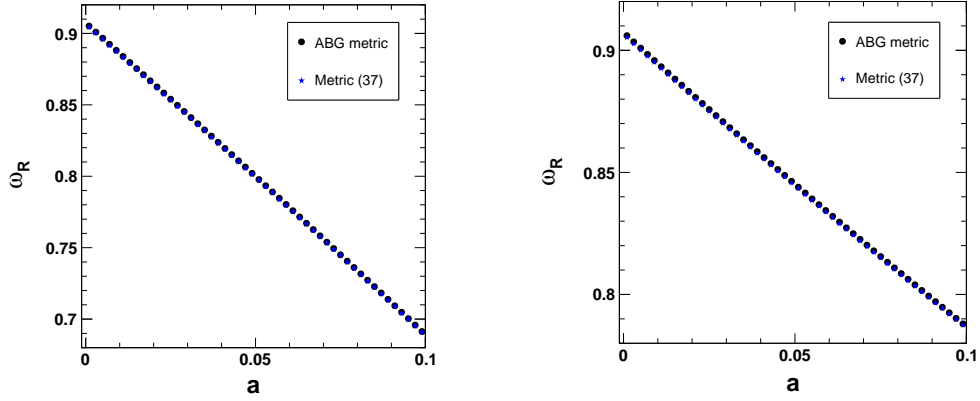


FIG. 13: Real QNMs versus cloud of strings parameter  $a$  for the ABG black hole and the black hole defined in Eq. (40) with  $n = 0$ ,  $l = 4$ ,  $q = 0.5$ ,  $M = 1$ ,  $\zeta = -0.4$  and  $\beta = 0.1$  (on left panel), and  $\beta = -0.1$  (on right panel).

In Fig. 14, imaginary QNMs are plotted with respect to  $a$  for both the black holes with  $q = 0.5$ ,  $M = 1$ ,  $\zeta = -0.4$  and  $\beta = 0.1$  (on left panel), and  $\beta = -0.1$  (on right panel). Here, the magnitude of the imaginary quasinormal frequencies,  $\omega_I$  decreases more rapidly with  $a$  for  $\beta = 0.1$  showing the less damping. As in case of the real quasinormal frequencies, here also the variation of frequencies with respect to  $a$  is almost linear. These results show that the GWs decay slowly with increase in the cloud of strings parameter  $a$ . This result is consistent with a recent study, where the authors have considered a Schwarzschild black hole in Rastall gravity surrounded by a cloud of strings [49].

In Fig. 15 we have plotted  $\omega_R$  versus  $\beta$  (on left panel) and  $\omega_I$  versus  $\beta$  (on right panel) with  $q = 0.8$ ,  $M = 1$ ,  $\zeta = -0.4$  and  $a = 0.1$  for both of the black holes. Here in case of real frequencies, with increase in  $\beta$ ,  $\omega_R$  increases and reaches a maximum value at  $\beta$  around  $-0.1$  and then again starts to decrease for both of the black holes. Similarly, in case of  $\omega_I$ , the magnitude increases with increase in  $\beta$  and reaches a maximum value at around  $-0.15$ . The second black hole seems to be more sensitive in terms of both  $\omega_R$  and  $\omega_I$  for the considered set of parameters. In both the plots,  $\beta = 0$  corresponds to GR limit and it can be seen that in Rastall gravity, depending on the value of Rastall parameter  $\beta$  QNMs can be greater or less than the corresponding



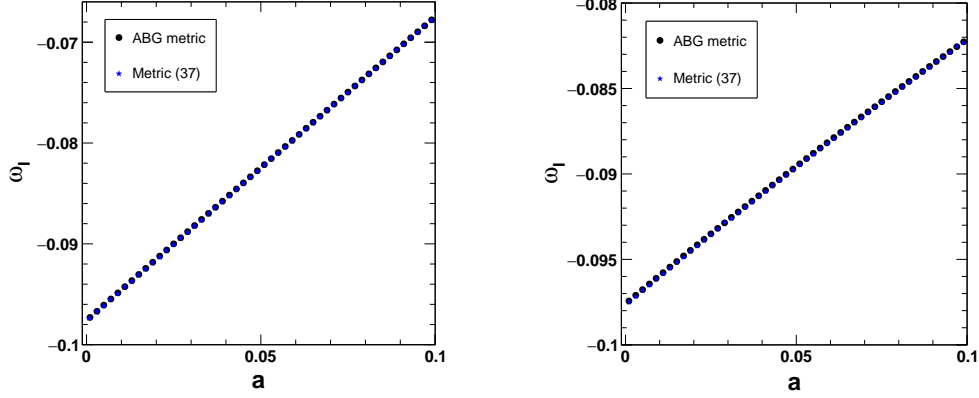


FIG. 14: Behaviour of Imaginary QNMs with respect to the cloud of strings parameter  $a$  for the ABG black hole and the black hole defined in Eq. (40) with  $n = 0, l = 4, q = 0.5, M = 1, \zeta = -0.4$  and  $\beta = 0.1$  (on left panel), and  $\beta = -0.1$  (on right panel).

GR values with an upper bound on the magnitude of quasinormal frequencies. However, this upper bound depends on the other parameters also. Another observation in this case is that for the second black hole i.e. black hole defined by our metric (40), the magnitude of quasinormal frequencies are greater than the ABG black hole. But in Table I, we observed an opposite scenario. It is due to the fact that here we have considered a higher value of  $q$  and  $\zeta$ . From the previous part, we have seen that  $\zeta$  can be more sensitive to potential and hence QNMs for higher values of  $q$ . So, these results apparently suggest that an increase in  $\zeta$  might increase the real quasinormal frequencies. To see this clearly, we have plotted real QNMs versus  $\zeta$  for a positive and negative  $\beta$  value in Fig. 16. The figure shows that with increase in  $\zeta$ ,  $\omega_R$  increases linearly. Also we found that the slope of the curve increases with increase in the value of  $q$ . The magnitude of  $\omega_I$  decreases with increase in  $\zeta$  for both positive and negative values of  $\beta$  (see Fig. 17). However,  $\zeta$  is less sensitive to  $\omega_I$  in comparison to  $\omega_R$ . These results suggest that with increase in  $\zeta$ , gravitational waves decay slowly. Again in case of  $\beta$ , GWs decay rapidly up to  $\beta \sim -0.15$  and beyond this value, GWs start to decay slowly (see Fig. 15).

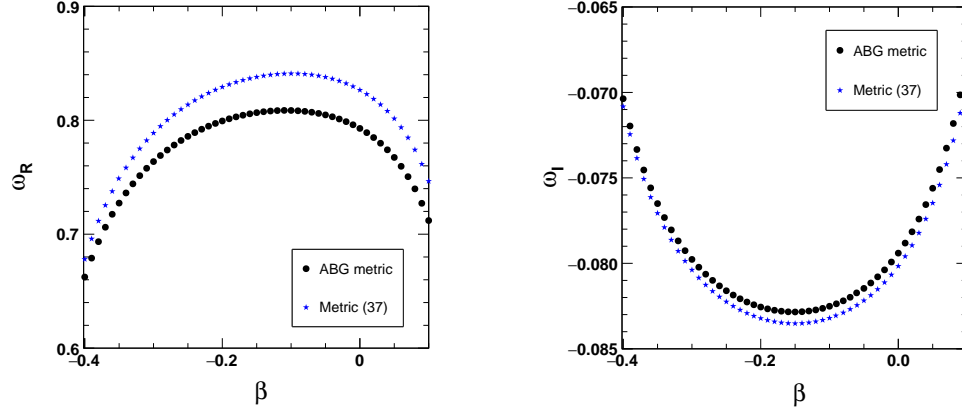


FIG. 15: Variation of QNMs in terms of  $\beta$  for the ABG black hole and the black hole defined in Eq. (40) with  $n = 0, l = 4, q = 0.8, M = 1, \zeta = -0.4$  and  $a = 0.1$ .

Finally, we observed the variation of  $\omega_R$  and  $\omega_I$  with respect to  $q$  for both the black holes in Fig. 18 with  $\beta = 0.05, M = 1, \zeta = -0.8$  and  $a = 0.1$ . QNMs for both the black holes are very close to each other in the asymptotic region i.e. for very small  $q$ . However, with increase in  $q$ , depending on the value of  $\zeta$ ,  $\omega_R$  as well as  $\omega_I$  for the second black hole starts deviating from the first one. In this case, for  $\zeta = -0.8$ , with increase in  $q$ ,  $\omega_R$  for the second black hole starts decreasing from the first one. In case of the imaginary quasinormal frequency, the magnitude of  $\omega_I$  increases for higher values of  $q$  for the second black hole. But for the first black hole, magnitude of  $\omega_I$  increases to a certain value and then starts to decrease towards  $q = 1$ . These results suggest that in case of the second black hole, GWs decay more rapidly than the ABG black hole when the charge  $q$  increases towards 1.

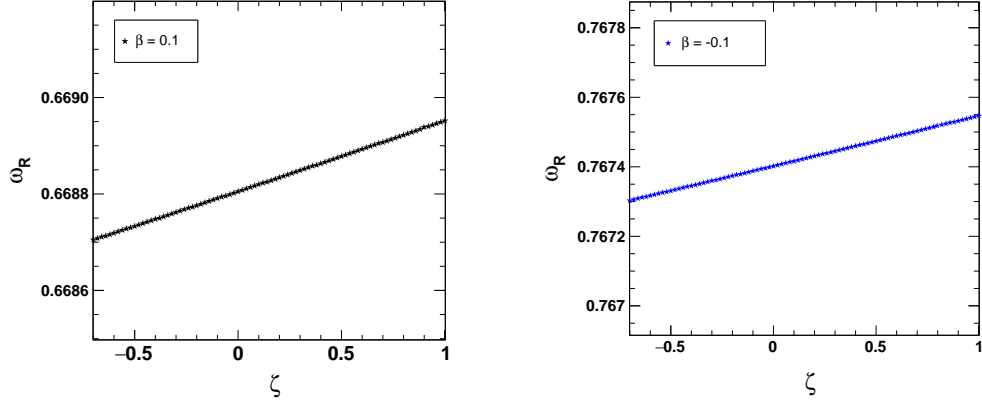


FIG. 16: Behaviour of real QNMs with respect to the model parameter  $\zeta$  for the black hole defined in Eq. (40) with  $n = 0$ ,  $l = 4$ ,  $q = 0.3$ ,  $M = 1$ ,  $a = 0.1$  and  $\beta = 0.1$  (on left panel), and  $\beta = -0.1$  (on right panel).

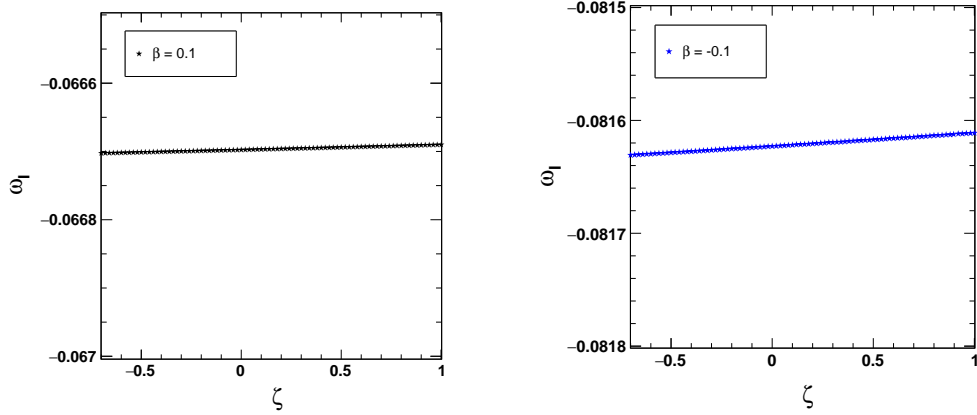


FIG. 17: Behaviour of imaginary QNMs with respect to the model parameter  $\zeta$  for the black hole defined in Eq. (40) with  $n = 0$ ,  $l = 4$ ,  $q = 0.3$ ,  $M = 1$ ,  $a = 0.1$  and  $\beta = 0.1$  (on left panel), and  $\beta = -0.1$  (on right panel).

#### IV. CHARACTERISTICS OF HAWKING TEMPERATURE OF THE BLACK HOLE SOLUTIONS

For both the black holes, from the metrics (29) and (40), we can calculate the event horizon radius using the condition:  $f(r_H) = 0$ , where  $r_H$  is the event horizon radius in general. For a general Schwarzschild black hole, this condition gives a simple relation between the mass and radius of the black hole. In our cases, the relation will be different from that of Schwarzschild and it will depend on the other metric function parameters also. In this section, we shall study the Hawking temperature of the black holes for different cases to have a visualization of the black hole characteristics. To do so, we obtain the surface gravity of the black holes by using definition:

$$\kappa_{r_H} = \frac{1}{2} \left. \frac{df(r)}{dr} \right|_{r=r_H}. \quad (52)$$

Here  $r_H = r_-, r_+$  and  $r_c$  for inner horizon or Cauchy horizon, event horizon and cloud of string horizon respectively. Using the surface gravity of a black hole one can easily obtain the Hawking temperature as

$$T_{BH} = \frac{\hbar \kappa_{r_H}}{2\pi}. \quad (53)$$

In Fig. 19 we have plotted the Hawking temperature  $T_{BH}$  with respect to cloud of string parameter  $a$  for the first horizon  $r_-$  (on the left panel) and for the second horizon  $r_+$  (on the right panel) for the ABG black hole with different values of black hole charge  $q$ . It is seen that for the  $r_-$ , the black hole temperature  $T_{BH}$  is negative and increases towards higher values of  $a$ . For the smaller charge  $q$ , the black hole temperature decreases drastically. But in case of second horizon  $r_+$ , the temperature  $T_{BH}$  is positive and it increases slowly with decrease in charge  $q$ . In this case,  $T_{BH}$  is a very small positive number and it decreases

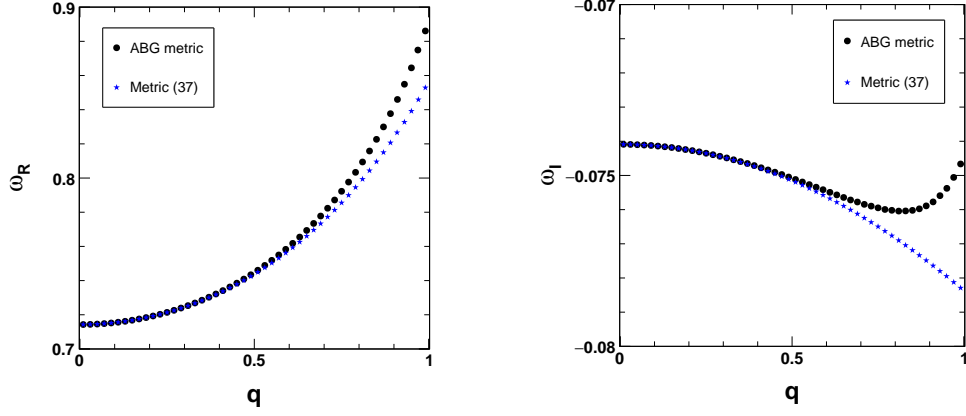


FIG. 18: Variation of QNMs with respect to  $q$  for the ABG black hole and the black hole defined in Eq. (40) with  $n = 0$ ,  $l = 4$ ,  $\beta = 0.05$ ,  $M = 1$ ,  $\zeta = -0.8$  and  $a = 0.1$ .

and moves towards zero with increase in surrounding field  $a$ . For large values of  $a$ , one can see that a variation in charge  $q$  does not show a significant changes in  $T_{BH}$ . Here, we have not plotted  $T_{BH}$  for the third horizon  $r_c$  as from our previous study of the black hole characteristics, it is clear that  $q$  has not any significant impact over the third horizon. However, one can see Fig. 21, which is plotted for  $r_c$  and shows that  $T_{BH}$  is again negative. In Fig. 20, we have plotted the Hawking temperature  $T_{BH}$  with respect to the cloud of string parameter  $a$  for the first horizon  $r_-$  (on the left panel) and for second horizon  $r_+$  (on the right panel) for the ABG black hole with different values of Rastall parameter  $\beta$ . In case of the first horizon  $r_-$ , we see that for smaller values of  $a$ , variation of  $\beta$  does not have any significant impacts on  $T_{BH}$ . However, with increase in  $a$ ,  $T_{BH}$  becomes more  $\beta$  dependent. This due to the fact that  $\beta$  is coupled with the cloud of string parameter  $a$  in the third term of the metric function. One can see that for the first horizon  $r_-$ , decrease in  $\beta$  increases  $T_{BH}$  for large  $a$ . A closer look shows that in the small  $a$  regime,  $T_{BH}$  slightly decreases with increase in  $a$  and for higher values of  $\beta$  this pattern continues. But in case of smaller values of  $\beta$ ,  $T_{BH}$  increases drastically with increase in  $a$ . In this case also,  $T_{BH}$  is negative. For the second horizon  $r_+$ , we observe an opposite scenario in comparison to the previous case. Here, for the small  $a$  regime,  $T_{BH}$  is almost indistinguishable for different values of  $\beta$ . However, for large  $a$ , smaller  $\beta$  has higher temperature  $T_{BH}$ . Finally, we plot  $T_{BH}$  with  $a$  for the third horizon  $r_c$  with different values of  $\beta$  in Fig. 21 as mentioned above. It is seen that  $T_{BH}$  is again negative here but with a very small magnitude. An increase in  $a$ , decreases  $T_{BH}$  further and for higher values of  $\beta$ ,  $T_{BH}$  decreases more drastically.

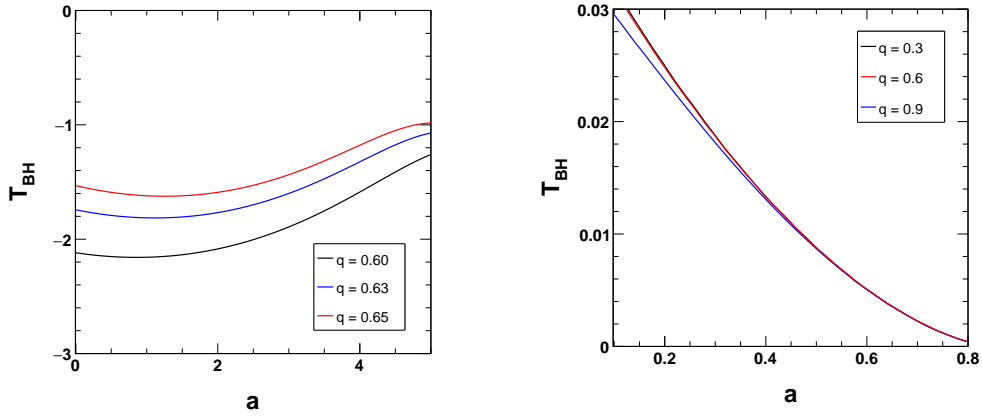


FIG. 19: Variation of  $T_{BH}$  with respect to  $a$  for different values of charge  $q$  for the first horizon  $r_-$  (on left panel) with  $M = 1$  and  $\beta = 0.1$ , and for the second horizon  $r_+$  (on right panel) with  $M = 1$  and  $\beta = 0.01$  in case of the ABG black hole.

Similarly, we have studied the variation of Hawking temperature  $T_{BH}$  with respect to the cloud of strings parameter  $a$  for the black hole defined by the metric (40). In Fig. 22 we have plotted the Hawking temperature  $T_{BH}$  versus the cloud of strings parameter  $a$  for the first horizon  $r_-$  (on the left panel) and for the second horizon  $r_+$  (on the right panel) for different values of  $\beta$ . In both cases,  $T_{BH}$  decreases with increase in cloud of strings parameter  $a$ . For higher values of  $\beta$ ,  $T_{BH}$  has smaller values corresponding to non-zero  $a$  values. For the first case,  $T_{BH}$  is negative and for the second case, it is a small positive number close to zero. From the previous study of the metric function, it is clear that the Rastall parameter  $\beta$  has a significant impact over

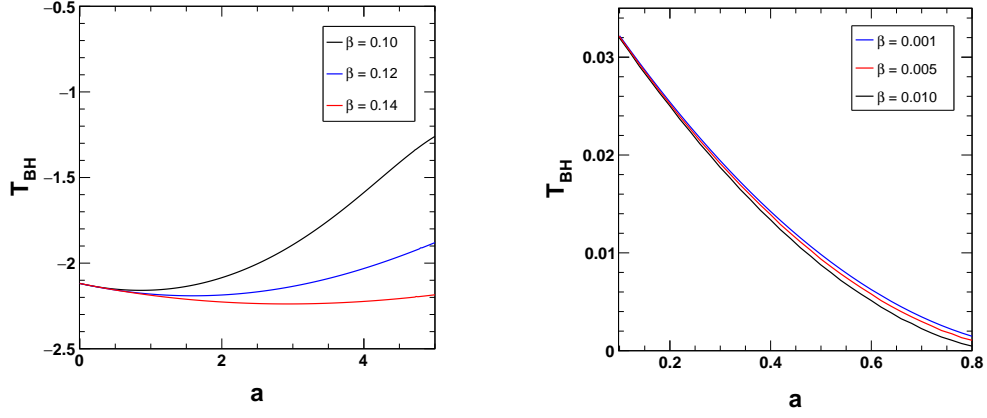


FIG. 20: Variation of  $T_{BH}$  versus  $a$  for different values of  $\beta$  for the first horizon  $r_-$  (on left panel) with  $M = 1$  and  $q = 0.6$ , and for the second horizon  $r_+$  (on right panel) with  $M = 1$  and  $q = 0.3$  in case of the ABG black hole.

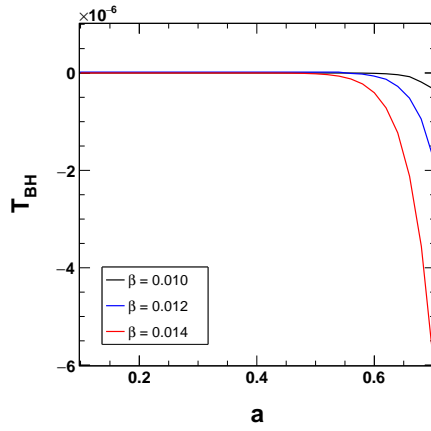


FIG. 21: Variation of  $T_{BH}$  with respect to  $a$  for different values of  $\beta$  for the third horizon or cloud of string horizon  $r_c$  with  $M = 1$  and  $q = 0.6$  in case of the ABG black hole.

the third horizon  $r_c$  of the black hole. This suggests that  $T_{BH}$  corresponding to the third horizon will show noticeable changes for different values of  $\beta$ . This variation can be seen in Fig. 23. For  $\beta = 0.10$ ,  $T_{BH}$  decreases upto  $a = 0.28$  and then suddenly increases and approaches to zero at around  $a = 0.311029183$ . For the considered parameter set, i.e. for  $M = 1$ ,  $q = 0.6$ ,  $\zeta = -0.4$  and  $\beta = 0.10$ , when  $a$  approaches 0.311029183, the third horizon  $r_c$  and the second horizon  $r_+$  coincide to give a single horizon. Beyond this critical point, both  $r_+$  and  $r_c$  start to vanish. From the figure, it is also clearly seen that this critical  $a$  value increases with decrease in  $\beta$ . In Fig. 24, we have plotted  $T_{BH}$  with respect to  $a$  for different values of  $q$  in case of  $r_-$  and  $r_+$ . We see that for  $r_-$ ,  $T_{BH}$  decreases with increase in  $a$  and higher charge  $q$  has higher  $T_{BH}$  values. In case of  $r_+$ , it is seen that  $T_{BH}$  decreases and approaches zero with increase in  $a$ . But here we observe a junction point for some  $a$  at which  $T_{BH}$  for all  $q$  coincides and flips the variation pattern. This is clearly seen from the right panel of this figure, where for  $q = 0.9$ ,  $T_{BH}$  is smaller than the other two cases with  $q = 0.5$  and  $0.1$  in the small  $a$  regime. But as  $a$  increases, we observe an opposite pattern. Finally, in Fig. 25, we have plotted  $T_{BH}$  with respect to  $a$  for different values of  $\zeta$  for  $r_-$  and  $r_+$  respectively. For  $r_-$ , the behaviour is almost identical to the previous case with different values of  $q$ . But in case of  $r_+$  we observe a slightly different pattern for small  $a$  regime with higher  $\zeta$  value. But towards higher values of  $a$ ,  $\zeta$  dependency of  $T_{BH}$  ceases and the graphs become almost indistinguishable.

Thus for both the black holes we see that for the first and the third horizon,  $T_{BH}$  is negative which is an anomalous behaviour. This is actually not a new outcome for a black hole in modified gravity as it was encountered earlier also [72–75]. In Ref. [72], the possibility of negative Hawking temperatures of black holes was shown with some added matter-energy content, for example quintessence, higher dimensional spacetimes and MTGs. In a recent study [73], it was mentioned that the Hawking temperature can be negative for quintessence and cloud of strings fields. Therefore our result resonates these earlier observations in case of Hawking temperature.

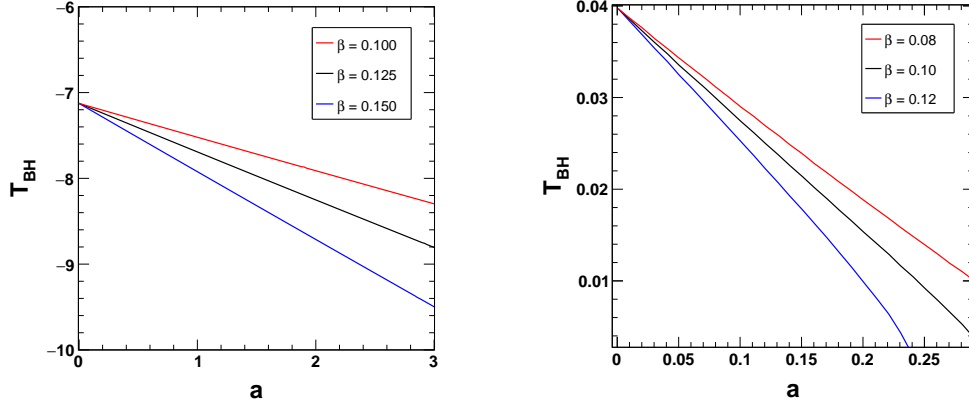


FIG. 22:  $T_{BH}$  versus  $a$  for the first horizon  $r_-$  (on left panel) with  $M = 1$ ,  $q = 0.6$  and  $\zeta = -0.4$ , and for the second horizon  $r_+$  (on right panel) with  $M = 1$ ,  $q = 0.3$  and  $\zeta = -0.8$  for the black hole defined by the metric (40).

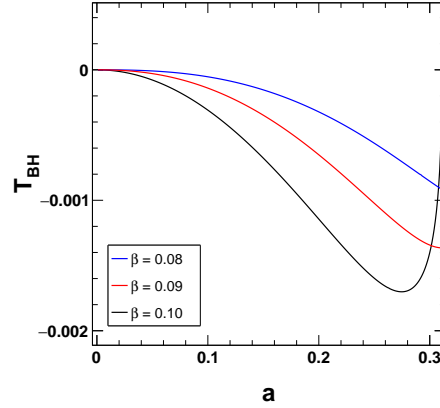


FIG. 23:  $T_{BH}$  with respect to  $a$  for the third horizon or cloud of string horizon  $r_c$  with parameters  $M = 1$ ,  $q = 0.6$  and  $\zeta = -0.4$  for the black hole defined by the metric (40).

## V. CONCLUSION

In this work, we have studied the QNMs and properties of the ABG black hole and a new black hole surrounded by a cloud of strings field in Rastall gravity. The main motivation of this study is to show the dependency of QNMs and black hole characteristics on the non-linear charge distribution surrounded by a cloud of string field in Rastall gravity. Recently a study has been done in Ref. [49], where the authors studied the QNMs and spectroscopy of a Schwarzschild black hole in Rastall gravity. But in our work we have considered the Reissner-Nordström black hole in Rastall gravity surrounded by a cloud of strings in Rastall gravity at first and then we have extended the black hole metric to non-linear charge distribution by considering the ABG black hole and a new black hole. The main characteristic of ABG black hole is that it gives a regular black hole in GR surrounded by a cloud of strings. But in case of Rastall gravity, the cloud of strings parameter is coupled with the Rastall parameter in the black hole metric function giving a possibility of singularity from the last term of the metric function. However, we have found that this issue can be resolved by setting  $0.25 < \beta < 0.50$ . Thus, we have shown that by controlling the Rastall parameter it is still possible to have a regular black hole in this case also. Inspired from the ABG black hole, we have introduced a new black hole with a different charge distribution function and with an extra model parameter  $\zeta$ . This parameter can control the singularity arising from the charge and mass coupled term in the metric function. We found that  $\zeta = \text{arcCsch}(1) = 0.881374$  and  $0.25 < \beta < 0.50$  can make the second black hole a regular one. The main advantage of using this new parameter is that for the ABG black hole, in GR, we always get a regular black hole, but in case of the second black hole, in GR, only  $\zeta = \text{arcCsch}(1) = 0.881374$  can give a regular black hole. For other cases, the black hole has a physical singularity.

We have also shown that both the black holes behave identically in the asymptotic regime. But with increase in charge  $q$ , the black holes start to deviate from each other. In case of QNMs also we have observed the same results. However, the

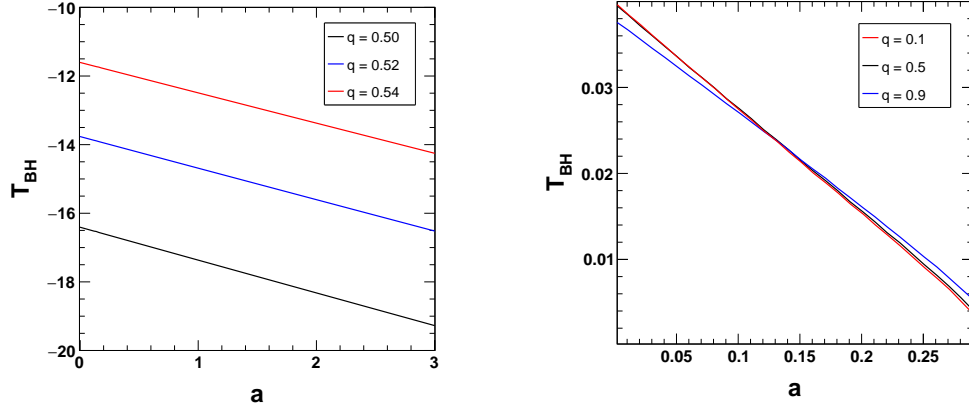


FIG. 24: Behaviour of  $T_{BH}$  with respect to  $a$  for the first horizon  $r_-$  (on left panel), and for the second horizon  $r_+$  (on right panel) with parameters  $M = 1$ ,  $\beta = 0.1$  and  $\zeta = -0.4$  for the black hole defined by the metric (40).

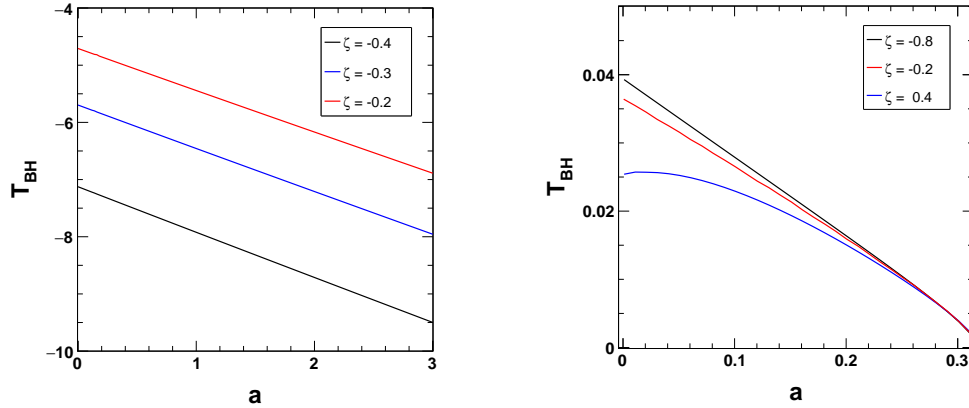


FIG. 25: Variation of  $T_{BH}$  in terms of  $a$  for the first horizon  $r_-$  (on left panel) with parameters  $M = 1$ ,  $\beta = 0.1$  and  $q = 0.6$ , and for the second horizon  $r_+$  (on right panel) with parameters  $M = 1$ ,  $\beta = 0.1$  and  $q = 0.9$  for the black hole defined by the metric (40).

free parameter  $\zeta$  can be controlled to adjust the black hole properties and QNMs up to some extent. Due to this property, such a model can be easily fitted with experimental results. Thus there is a good possibility of physical consistency with the experimental constraints on the QNMs in case of the second black hole.

In a recent work, QNMs of black holes with a non-linear charge distribution in Rastall gravity surrounded by dark energy fields have been studied [22]. We observe that the dependency of QNMs with the Rastall parameter studied in that work is completely different from this work. Hence, the impact of the cloud of strings parameter and the dark energy fields on the QNMs is not identical.

We believe that the impacts of the cloud of strings on the black holes in Rastall gravity can be studied more explicitly in the near future. Specially an anisotropic cloud of strings field in extended Rastall gravity can shed more light on the dependency of different properties of the black holes including QNMs with these situations.

- 
- [1] C. M. Will, *The Confrontation between General Relativity and Experiment*, *Living Rev. Relativ.* **17**, 4 (2014) [arXiv:gr-qc/0510072].
  - [2] R. A. Hulse and J. H. Taylor, *Discovery of a Pulsar in a Binary System*, *ApJL* **195**, L51 (1975).
  - [3] T. Damour and J. H. Taylor, *Strong-Field Tests of Relativistic Gravity and Binary Pulsars*, *Phys. Rev. D* **45**, 1840 (1992).
  - [4] B. P. Abbott et al., *Observation of Gravitational Waves from a Binary Black Hole Merger*, *Phys. Rev. Lett.* **116**, 061102 (2016).
  - [5] B. P. Abbott et al., *Observation of Gravitational Waves from a 22-Solar-Mass Binary Black Hole Coalescence*, *Phys. Rev. Lett.* **116**, 241103 (2016).
  - [6] B. P. Abbott et al., *Search for transient gravitational waves in coincidence with short-duration radio transients during 2007-2013*, *Phys. Rev. D* **93**, 122008 (2016).

- [7] B. P. Abbott et al., *First narrow-band search for continuous gravitational waves from known pulsars in advanced detector data*, *Phys. Rev. D* **96**, 122006 (2017).
- [8] B. P. Abbott et al., *Observation of Gravitational Waves from a Binary Neutron Star Inspiral*, *Phys. Rev. Lett.* **119**, 161101 (2017).
- [9] E. Burns et al., *A Fermi Gamma-Ray Burst Monitor Search for Electromagnetic Signals Coincident with Gravitational-wave Candidates in Advanced LIGO's First Observing Run*, *ApJ* **87**, 1 (2019).
- [10] B. P. Abbott et al., *Observation of a Binary-Black-Hole Coalescence with Asymmetric Masses*, *Phys. Rev. D* **102**, 043015 (2020).
- [11] R. Abbott et al., *Observation of Gravitational Waves from Two Neutron Star–Black Hole Coalescences*, *ApJL* **915**, L5 (2021).
- [12] A. G. Riess et al., *Observational Evidence from Supernovae for an Accelerating Universe and a Cosmological Constant*, *The Astronomical Journal* **116**, 1009 (1998).
- [13] S. Perlmutter et al., *Measurements of  $\Omega$  and  $\Lambda$  from 42 High-Redshift Supernovae*, *ApJ* **517**, 565 (1999).
- [14] K. S. Stelle, *Renormalization of Higher-Derivative Quantum Gravity*, *Phys. Rev. D* **16**, 953 (1977).
- [15] N. A. Bahcall, *The Cosmic Triangle: Revealing the State of the Universe*, *Science* **284**, 1481 (1999).
- [16] C. Pérez de los Heros, *Status, Challenges and Directions in Indirect Dark Matter Searches*, *Symmetry* **12**, 1648 (2020).
- [17] P. Bull et al., *Beyond  $\Lambda$ CDM: Problems, Solutions, and the Road Ahead*, *Physics of the Dark Universe* **12**, 56 (2016).
- [18] L. Amendola and S. Tsujikawa, *Dark Energy: Theory and Observations* (Cambridge University Press, Cambridge, 2010).
- [19] E. J. Copeland, M. Sami, and S. Tsujikawa, *Dynamics of Dark Energy*, *Int. J. Mod. Phys. D* **15**, 1753 (2006).
- [20] D. J. Gogoi and U. Dev Goswami, *Gravitational Waves in  $f(\mathbf{R})$  Gravity Power Law Model*, *Indian J. Phys.* (2021).
- [21] M. C. Miller and N. Yunes, *The New Frontier of Gravitational Waves*, *Nature* **568**, 469 (2019).
- [22] D. J. Gogoi and U. Dev Goswami, *Quasinormal Modes of Black Holes with Non-Linear-Electrodynamics Sources in Rastall Gravity*, *Physics of the Dark Universe* **33**, 100860 (2021).
- [23] D. J. Gogoi and U. Dev Goswami, *A New  $f(\mathbf{R})$  Gravity Model and Properties of Gravitational Waves in It*, *Eur. Phys. J. C* **80**, 1101 (2020).
- [24] J. M. Ezquiaga and M. Zumalacá regui, *Dark Energy in Light of Multi-Messenger Gravitational-Wave Astronomy*, *Front. Astron. Space Sci.* **5**, 44 (2018).
- [25] B. P. Abbott et al., *GW170104: Observation of a 50-Solar-Mass Binary Black Hole Coalescence at Redshift 0.2*, *Phys. Rev. Lett.* **118**, 221101 (2017).
- [26] P. Rastall, *Generalization of the Einstein Theory*, *Phys. Rev. D* **6**, 3357 (1972).
- [27] W. A. G. De Moraes and A. F. Santos, *Lagrangian Formalism for Rastall Theory of Gravity and Gödel-Type Universe*, *Gen. Relativ. Gravit.* **51**, 167 (2019).
- [28] H. Shabani and A. Hadi Ziaie, *A Connection between Rastall-Type and  $f(\mathbf{R}, T)$  Gravities*, *EPL* **129**, 20004 (2020).
- [29] M. Visser, *Rastall Gravity Is Equivalent to Einstein Gravity*, *Phys. Lett. B* **782**, 83 (2018)[arXiv:1711.11500].
- [30] F. Darabi, H. Moradpour, I. Licata, Y. Heydarzade, and C. Corda, *Einstein and Rastall Theories of Gravitation in Comparison*, *Eur. Phys. J. C* **78**, 25 (2018).
- [31] A. H. Ziaie, H. Moradpour, and S. Ghaffari, *Gravitational Collapse in Rastall Gravity*, *Phys. Lett. B* **793**, 276 (2019).
- [32] Y. Heydarzade and F. Darabi, *Black Hole Solutions Surrounded by Perfect Fluid in Rastall Theory*, *Phys. Lett. B* **771**, 365 (2017).
- [33] Y. Heydarzade, H. Moradpour, and F. Darabi, *Black Hole Solutions in Rastall Theory*, *Can. J. Phys.* **95**, 1253 (2017).
- [34] R. Kumar and S. G. Ghosh, *Rotating Black Hole in Rastall Theory*, *Eur. Phys. J. C* **78**, 750 (2018).
- [35] C. E. M. Batista, M. H. Daouda, J. C. Fabris, O. F. Piattella, and D. C. Rodrigues, *Rastall Cosmology and the  $\Lambda$ CDM Model*, *Phys. Rev. D* **85**, 084008 (2012).
- [36] H. Moradpour, Y. Heydarzade, F. Darabi, and I. G. Salako, *A Generalization to the Rastall Theory and Cosmic Eras*, *Eur. Phys. J. C* **77**, 259 (2017).
- [37] A. S. Al-Rawaf and M. O. Taha, *A Resolution of the Cosmological Age Puzzle*, *Phys. Lett. B* **366**, 69 (1996).
- [38] A. S. Al-Rawaf and M. O. Taha, *Cosmology of General Relativity without Energy-Momentum Conservation*, *Gen. Relat. Gravit.* **28**, 935 (1996).
- [39] J. C. Fabris, R. Kerner, and J. Tossa, *Perturbative analysis of generalized Einstein theories*, *Int. J. Mod. Phys. D* **09**, 111 (2000).
- [40] A.-M. M. Abdel-Rahman and M. H. A. Hashim, *Gravitational Lensing in A Model With Non-Interacting Matter and Vacuum Energies*, *Astrophys. Space Sci.* **298**, 519 (2005).
- [41] A.-M. M. Abdel-Rahman, *Gravitational Lensing Effects in a Modified General Relativity Model*, *Astrophys. Space Sci.* **278**, 385 (2001).
- [42] H. Moradpour, N. Sadeghnezhad, and S. H. Hendi, *Traversable Asymptotically Flat Wormholes in Rastall Gravity*, *Can. J. Phys.* **95**, 1257 (2017).
- [43] J. C. Fabris, T. C. da C. Guio, M. H. Daouda, and O. F. Piattella, *Scalar Models for the Generalized Chaplygin Gas and the Structure Formation Constraints*, *Gravit. Cosmol.* **17**, 259 (2011).
- [44] T. Caramês et al., *A Rastall Scalar-Tensor theory*, (2015), [arXiv:1503.04882].
- [45] T. R. P. Caramês et al., *The Brans–Dicke–Rastall Theory*, *Eur. Phys. J. C* **74**, 3145 (2014).
- [46] L. Perivolaropoulos, *PPN Parameter  $\gamma$  and Solar System Constraints of Massive Brans-Dicke Theories*, *Phys. Rev. D* **81**, 047501 (2010).
- [47] J. de M. Toledo and V. B. Bezerra, *Black Holes with Cloud of Strings and Quintessence in Lovelock Gravity*, *Eur. Phys. J. C* **78**, 534 (2018).
- [48] A. Ali, *Magnetic Lovelock Black Holes with a Cloud of Strings and Quintessence*, *Int. J. Mod. Phys. D* **30**, 2150018 (2021).
- [49] X.-C. Cai and Y.-G. Miao, *Quasinormal Modes and Spectroscopy of a Schwarzschild Black Hole Surrounded by a Cloud of Strings in Rastall Gravity*, *Phys. Rev. D* **101**, 104023 (2020).
- [50] E. Ayón-Beato and A. García, *New Regular Black Hole Solution from Nonlinear Electrodynamics*, *Phys. Lett. B* **464**, 25 (1999).
- [51] K. D. Kokkotas and B. G. Schmidt, *Quasi-Normal Modes of Stars and Black Holes*, *Living Rev. Relativ.* **2**, 2 (1999).
- [52] C. V. Vishveshwara, *Stability of the Schwarzschild Metric*, *Phys. Rev. D* **1**, 2870 (1970).
- [53] W. H. Press, *Long Wave Trains of Gravitational Waves from a Vibrating Black Hole*, *ApJ* **170**, L105 (1971).
- [54] S. Chandrasekhar and S. Detweiler, *The Quasi-Normal Modes of the Schwarzschild Black Hole*, *Proc. R. Soc. Lond. A* **344**, 441 (1975).

- [55] E. Berti et al., *Testing General Relativity with Present and Future Astrophysical Observations*, *Class. Quantum Grav.* **32**, 243001 (2015).
- [56] O. Dreyer et al., *Black-Hole Spectroscopy: Testing General Relativity through Gravitational-Wave Observations*, *Class. Quantum Grav.* **21**, 787 (2004).
- [57] A. M. Oliveira, H. E. S. Velten, J. C. Fabris and L. Casarini, *Neutron Stars in Rastall Gravity*, *Phys. Rev. D* **92**, 044020 (2015)[arXiv:1506.00567].
- [58] R. Kumar, B. P. Singh, M. S. Ali, and S. G. Ghosh, *Shadows of Black Hole Surrounded by Anisotropic Fluid in Rastall Theory*, *Physics of the Dark Universe* **34**, 100881 (2021).
- [59] S. Chen and J. Jing, *Quasinormal modes of a black hole surrounded by quintessence*, *Class. Quantum Grav.* **22**, 4651 (2005)[arXiv:gr-qc/0511085].
- [60] Y. Zhang and Y.X. Gui, *Quasinormal modes of gravitational perturbation around a Schwarzschild black hole surrounded by quintessence*, *Class. Quantum Grav.* **23**, 6141 (2006)[arXiv:gr-qc/0612009].
- [61] Y. Zhang, Y.X. Gui and F. Li, *Quasinormal modes of a Schwarzschild black hole surrounded by free static spherically symmetric quintessence: electromagnetic perturbations*, *Gen. Relativ. Gravit.* **39**, 1003 (2007)[arXiv:gr-qc/0612010].
- [62] J. Liang, *Quasinormal Modes of the Schwarzschild Black Hole Surrounded by the Quintessence Field in Rastall Gravity*, *Commun. Theor. Phys.* **70**, 695 (2018).
- [63] L. Balart and E. C. Vagenas, *Regular Black Holes with a Nonlinear Electrodynamics Source*, *Phys. Rev. D* **90**, 124045 (2014) [arXiv:1408.0306].
- [64] S. Nojiri and S. D. Odintsov, *Regular multihorizon black holes in modified gravity with nonlinear electrodynamics*, *Phys. Rev. D* **96**, 104008 (2017).
- [65] K. Jusufi, M. Amir, M. S. Ali, and S. D. Maharaj, *Quasinormal Modes, Shadow, and Greybody Factors of 5D Electrically Charged Bardeen Black Holes*, *Phys. Rev. D* **102**, 064020 (2020).
- [66] P. S. Letelier, *Clouds of Strings in General Relativity*, *Phys. Rev. D* **20**, 1294 (1979).
- [67] K. K. J. Rodrigue, M. Saleh, B. B. Thomas, and T. C. Kofane, *Thermodynamics Phase Transition and Hawking Radiation of the Schwarzschild Black Hole with Quintessence-like Matter and a Deficit Solid Angle*, *Gen Relativ Gravit* **50**, 52 (2018).
- [68] P. Xi, *Quasinormal Modes of a Black Hole with Quintessence-like Matter and a Deficit Solid Angle: Scalar and Gravitational Perturbations*, *Astrophys Space Sci* **321**, 47 (2009).
- [69] V. Ferrari and L. Gualtieri, *Quasi-Normal Modes and Gravitational Wave Astronomy*, *Gen. Relativ. Gravit.* **40**, 945 (2008) [arXiv:0709.0657].
- [70] R. A. Konoplya, *Quasinormal Behavior of the D -Dimensional Schwarzschild Black Hole and the Higher Order WKB Approach*, *Phys. Rev. D* **68**, 024018 (2003).
- [71] R. A. Konoplya, A. Zhidenko, and A. F. Zinhailo, *Higher Order WKB Formula for Quasinormal Modes and Grey-Body Factors: Recipes for Quick and Accurate Calculations*, *Class. Quantum Grav.* **36**, 155002 (2019).
- [72] M.-I. Park, *Can Hawking Temperatures Be Negative?*, *Phys. Lett. B* **663**, 259 (2008).
- [73] J. M. Toledo and V. B. Bezerra, *Kerr-Newman-AdS Black Hole with Quintessence and Cloud of Strings*, *Gen. Relativ. Gravit.* **52**, 34 (2020).
- [74] T. Ibungochouba Singh, Y. K. Meitei, and I. A. Meitei, *Effect of GUP on Hawking Radiation of BTZ Black Hole*, *Int. J. Mod. Phys. A* **35**, 2050018 (2020).
- [75] Y.-H. Wei and Z.-H. Chu, *Thermodynamic Properties of a Reissner-Nordström Quintessence Black Hole*, *Chinese Phys. Lett.* **28**, 100403 (2011).